



**TECHNISCHE
UNIVERSITÄT
DRESDEN**

Fakultät Maschinenwesen Institut für Festkörpermechanik
Professur für Mechanik multifunktionaler Strukturen

Design and Simulation of an Astro-Photography Tripod with Hydrogel Actuator

Shantesh Rai

CMS-CE

D.o.B. [REDACTED]

Matriculation Number [REDACTED]

Master Thesis

Supervisor

Dr.-Ing. Adrian Ehrenhofer

Supervising Professor

Prof. Dr.-Ing. Thomas Wallmersperger

Declaration of Authorship

I hereby declare that the research work submitted today on 19/07/2022 to the Institute of Solid Mechanics with the title,

Design and Simulation of an Astro-Photography Tripod with Hydrogel Actuators

was independently authored by me and no other resources except the ones mentioned were used and that all citations were correctly labeled.

Dresden, 19.07.22

A black rectangular box redacting the signature of the author.

Signature

Assignment for the Master Thesis

Course of Studies Computational Modeling and Simulation

Track Computational Engineering

Student's Name Shantesh Rai

Topic: Design and simulation of an astro-photography tripod with hydrogel actuators

Background:

Hydrogels are polymers that can swell and deswell in water, when subjected to a stimulus change. The resulting large deformation of the material is very slow and the water as well as the stimulus have to be provided to allow the application as actuators.

Task description and deliverables:

In the current work, a tripod system has to be designed that allows an adequate tracking of the night sky. The design is based on a literature review about the application and function of hydrogels (Milestone M1). In Milestone M2, the system's design based on analytical derivations of forces, rotation velocities and dimensions is completed. Then, the actuator will be modelled using the Finite-Element Software Abaqus and the Temperature-Expansion Model (M3).

Supervisor: Dr.-Ing. Adrian Ehrenhofer
Supervising Professor: Prof. Dr.-Ing. Thomas Wallmersperger

Start date: 28.02.2022
Submission Deadline: 01.08.2022



Prof. Dr.-Ing. habil. T. Wallmersperger
Supervising Professor

Table of Contents

1. Introduction.....	1
2. Hydrogel Application in Engineering: The What and The How.....	7
2.1 Introduction to hydrogels.....	7
2.2 Basic chemistry of swelling.....	9
2.2.1 Thermodynamics of hydrogel swelling.....	9
2.2.2 Kinetics of hydrogel swelling.....	11
2.3 Swelling Model.....	13
2.4 Methods of reducing the response time of hydrogels.....	15
2.5 Normalization of hydrogel swelling behaviour.....	16
2.6 Normalized Extended Temperature Expansion Model.....	19
2.7 Designing the Actuator for the Tripod.....	21
2.7.1 Assumptions, Constraints and Givens.....	21
2.7.2 Initial cylinder height.....	22
2.7.3 Cylinder diameter: Axial compressive load criteria.....	23
2.7.4 Cylinder diameter: Buckling criteria.....	24
2.7.5 Cylinder diameter: Bending criteria.....	24
2.7.6 Initial cylinder diameter.....	25
2.8 Finite Element Modelling and Simulation Setup.....	25
3. Results and Discussion.....	27
3.1 Simulation result and mesh convergence study.....	27
3.2 Design of the outer shell.....	29
3.3 Tripod: Elephant-leg design.....	30
3.4 Determinacy and Stability.....	31
3.5 Actuation in the tripod mechanism.....	34
3.6 Maximum deflection due to bending, and Critical load for buckling.....	35

3.7 Kinetics of the designed actuator.....	35
3.8 Constrained motion and strain-rate.....	36
4. Conclusion and Future-work.....	39
5. References.....	41

Table of Figures

Figure 1: Concept Design of Tripod.....	3
Figure 2: (Left) Example of Dobsonian mount. (Middle) Tripod Neck designed for this thesis. (Right) Commercially available generic tripod. Image source (Banas 2021).....	3
Figure 3: Tripod mechanism in action. The celestial body shows relative motion due to earth's rotation.....	4
Figure 4: Actuator in deswollen state (left) and swollen state (right).....	5
Figure 5: Commercial aquarium heater. Image source (Mylivell 2021).....	5
Figure 6: Acting forces on tripod legs.....	6
Figure 7: Stimuli-responsive hydrogel material. Image taken from Ehrenhofer (2018).....	8
Figure 8: Typical characteristic swelling curves of hydrogels. Image taken from Ehrenhofer (2018).....	8
Figure 9: Swelling curve of PNiPAAm hydrogel obtained from experimental data. Image taken from Ehrenhofer (2018).....	9
Figure 10: Two-step model of swelling mechanism. Image taken from Gerlach (2010).....	14
Figure 11: Procedure for Normalization of swelling behaviour. Image adopted from Ehrenhofer (2017).....	16
Figure 12: Comparison of different curve-fitting methods for data points. Image taken from Ehrenhofer (2017).....	17
Figure 13: (Left) Suitable for actuatoric application, (Right) Suitable for sensoric application. Image taken from Ehrenhofer (2018).....	18
Figure 14: Normalized swelling curves of six different hydrogel materials. Image taken from Ehrenhofer (2018).....	19
Figure 15: Evolution of NETEM model over the years. Image taken from Ehrenhofer (2020).....	20
Figure 16: Flowchart of design process for this thesis.....	21
Figure 17: Simulation model setup.....	26
Figure 18: Mesh convergence study.....	27
Figure 19: Displacement-time plot of the tracked point A.....	28
Figure 20: Actuator at initial state (left) and at final state (right).....	28

Figure 21: Left: Cross-section of concept design; Right: Cross-section of final shell design.....	30
Figure 22: Final tripod design: Elephant-leg Tripod.....	31
Figure 23: Topology plan of tripod mechanism.....	32
Figure 24: (Top two blocks) 3D Tripod structure and forces; (Middle) Normal leg and it's forces; (Last two Blocks) The segments of the actuated leg and the reaction forces acting on it.....	33
Figure 25: Actuation in tripod mechanism.....	34
Figure 26: Constraint Function.....	36
Figure 27: Strain rate of actuator as a function of rotation angle of the platform.....	37
Figure 28: Hydrogel swelling rate curves. Image source: (Left) (Mamidi 2019) , (Right) (Krause 2016).....	38

Table of Symbols and Abbreviations

Abbreviations		Symbols	
PNiPAAm	Poly(N-isopropyl acrylamide)	Q	Mass swelling ratio
PET	Polyethylene Terephthalate	q	Volume swelling ratio
NETEM	Normalized Extended Temperature Expansion Model	D_{coop}	Cooperative diffusion coefficient
FEM	Finite Element Method	t	time
LCST	Lower Critical Solution Temperature	τ	Characteristic swelling time
FH	Flory-Huggins theory	f	Correction term
RET	Rubber Elasticity Theory	T	Temperature
DLS	Dynamic Light Scattering	ϵ^H	Hencky strain
AR	Aspect Ratio	S	Stimulus
UV	Ultraviolet	$F^{Stimulus}$	Stimulus ratio
PCHIP	Piece-wise Cubic Hermite Inter-Polation splines	σ	Cauchy stress
TEM	Temperature Expansion Model	E	Modulus of Elasticity
ETEM	Extended Temperature Expansion Model	ρ	Density
CAD	Compter-Aided Design	h	Height (mm)
		d	Diameter (mm)
		l	Actuation length (mm)
		θ	Rotation angle (rad)
		β	Non-linear expansion coefficient
		δ	Beam deflection (mm)

1. Introduction

Astrophotography, also called astronomical imaging, is one of the oldest types of scientific photography wherein images of celestial bodies and events are captured (Ray 1999). There are many sub-fields within the domain of astrography each having a definite role, like stellar classification, star cartography, spectroscopy, astrometry, polarimetry, and discovery of astronomical bodies like comets, exoplanets, stars, meteors, supernovae, asteroids, etc. Malin et al. (Malin 2009) traces the inception of the development of astrophotography to the mid-19th century by amateur astronomers and experimenters. The earliest known endeavour in astrophotography was by a French artist and photographer Louis-Jacques-Mandé Daguerre in 1839, where he tried to capture a photo of the moon. However due to the tracking errors during the long exposure imaging, the image turned out to be a foggy spot.

Astrophotography is essentially done with long exposures, to accumulate as many photons from distant faint celestial objects as possible. This makes a tripod a necessary accessory as the camera needs to be still throughout the long capturing time, otherwise the image will have streaks of light or foggy spots (similar to what happened in 1839!). But the earth is continuously rotating with a constant velocity, which gives an apparent motion to the celestial bodies (known as diurnal motion). This again constraints the exposure time upto half a minute, after which light trails appear in the image. In order to get long exposures, the camera should be rotated to counter the diurnal motion, as explained in (Ashford 2022). This is realized by equatorial or computer-controlled altazimuth camera/telescope mounts. These mounts still have the limitation of tracking error which arises due to imperfections in gears of driving motor (called periodic error), sag in the telescope, and atmospheric refraction.

Smart materials have the ability to integrate actuatoric/sensoric functionality with structural functionality. Therefore, these can be used to make structures that have innate capability of actuation, eliminating external attachments like a motor. Hydrogel is one of such smart materials. These relatively unexplored materials have a huge untapped potential for application in various fields of engineering, medicine, etc. Due to their limited implementation in real-life, these materials tend to be unoptimized for new application. Hence, a lot of research work is done to find new areas for their use, assess the suitability and feasibility, and based on the findings optimize/customize the material property.

In line with the above discussed research trend in hydrogel application and also the shortcoming of tripod mounts, the idea to use hydrogel to make a tripod for astrophotography application was conceptualized. The ability of the hydrogel to produce

smooth, continuous and lag-free actuation further added to the motivation behind this thesis work.

Thus, the objective of this thesis work is to conceptualize, design, and model a tripod stand mechanism with the application of a thermo-sensitive hydrogel PNiPAAm, to produce the actuation needed for astrophotography purpose. Simulations will be conducted on the commercial numerical solver *ABAQUS* (*Dassault Systèmes*, 2022) for the designed actuator.

Due to the active-nature of the hydrogels, i.e. their capability to swell or deswell in response to an external stimulus, they have been used as actuators in many interesting engineering applications. Winkler (2020) presents a concept soft robotic system where active gel material was used to encapsulate rigid parts like batteries, electronics, etc. The design falls under the field of bio-mimicry, and the inspiration was drawn from animal organs which are encapsulated by skin/tissues/membranes. Such application of hydrogels create the possibility for robots to safely interact with humans. Membranes with permeation control were developed by coating PET membrane with hydrogel, as described in Ehrenhofer (2016). These membranes find application in microfluidics for biomedical use or chemical information processing. Yuk (2017) demonstrates a different method of hydrogel actuation for soft robotics application. Contrary to the prevalent methods where hydrogel produces an osmotic response by swelling/deswelling, the authors employed hydraulic actuation to the hydrogels eliminating hydrogel swelling phenomenon and alleviating the associated problem of slow response time and small output force. Sun (2012) details the synthesis of a hydrogel with enhanced toughness and stretchability. Krause (2016) delineates the synthesis of a bi-sensitive interpenetrating polymer network for microfluidic application. The authors report an improvement in swelling behaviour due to the presence of two different polymer networks. Swelling kinetics (see section 2.2.2) was also discussed for the used hydrogels and a correction factor was introduced in the cooperative diffusion coefficient to accommodate cylindrical geometries of arbitrary aspect ratio. Mazaheri (2019) developed an analytical model for hydrogels and then derived a second-order differential equation to implement the model in *ABAQUS* for finite element simulations. The developed analytical and numerical methods were then applied to assess the swelling characteristics of a hydrogel cylindrical shell. Ehrenhofer (2020) presents the designing of shell-forming structures with active hydrogels in combination with passive material layers. These active-passive composite structures find a potential application in flexible/rollable displays. A different swelling model combining expansion behaviour based on thermal expansion model with mechanical behaviour, called NETEM (refer section 2.6), is explained and implemented in *ABAQUS* to carry out finite element simulations.

This thesis work is the first work in this field of application and the resulting tripod model will act as a proof-of-concept. This calls for some assumptions and simplifications in the

model and experimental setup. Figure 1 shows the concept design of the tripod for this thesis. The mechanism design is inspired from the Dobsonian mount/telescope (Newton 1995). When combined with equatorial mounts, the Dobsonian mount becomes the subset of broad category of telescope mounts called Altazimuth mounts, which are two-axes mounts.

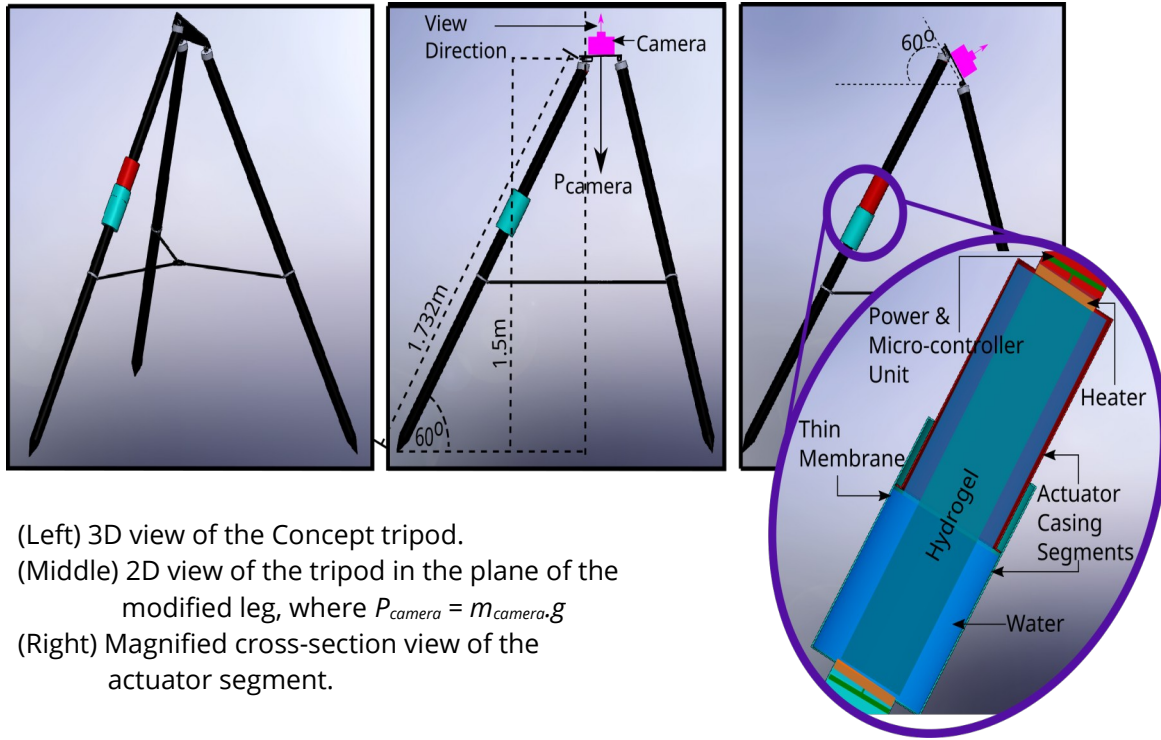


Figure 1: Concept Design of Tripod.



Figure 2: (Left) Example of Dobsonian mount. (Middle) Tripod Neck designed for this thesis. (Right) Commercially available generic tripod. Image source (Banas 2021).

The first assumption for the experimental setup was to place the tripod in earth's equatorial plane, so that the earth's polar axis is parallel to the only axis of rotation of the tripod. This will essentially fulfill the function of an equatorial mount. Second, the celestial object to be photographed is also located in the earth's equatorial plane and stationary, so that its apparent motion is a repercussion of earth's rotation only. Figure 3 represents the experimental setup assumed in this thesis work.

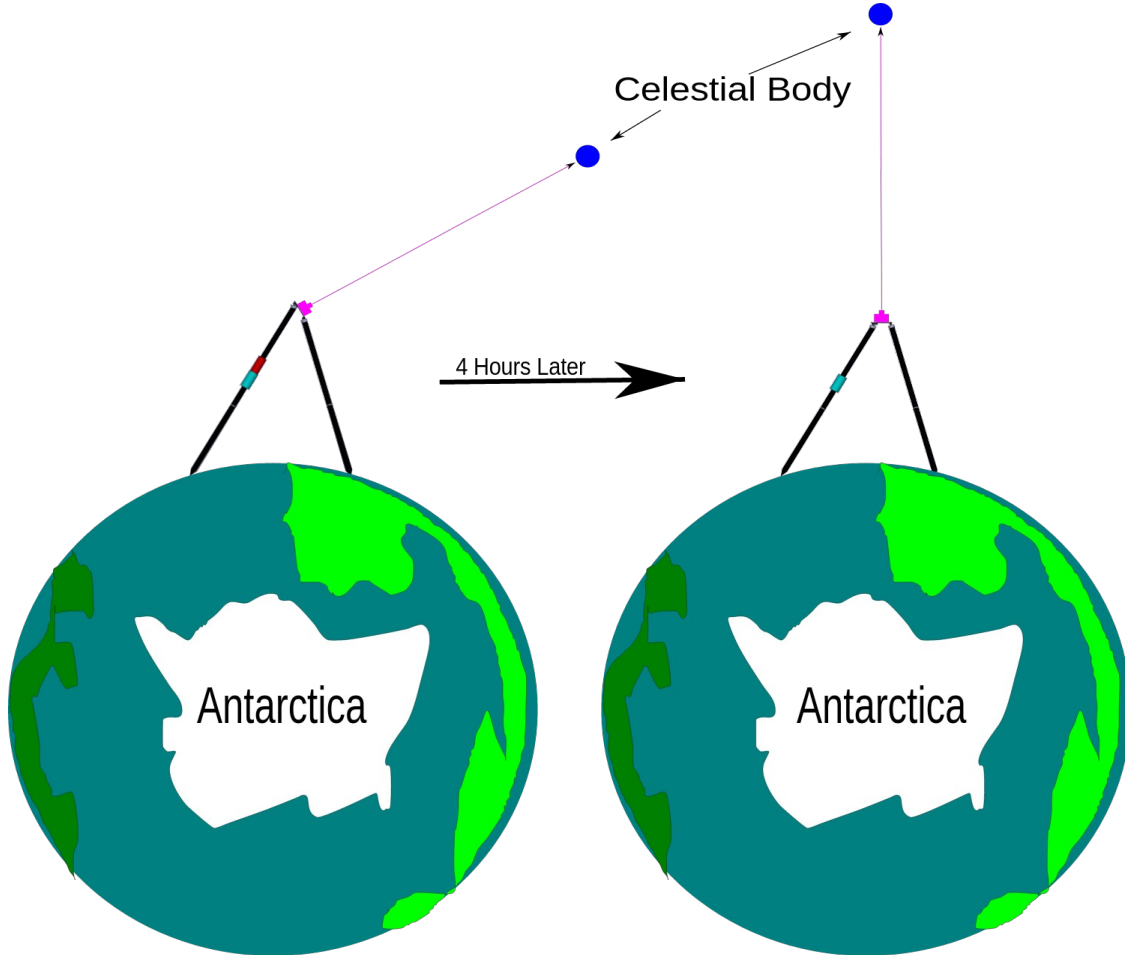


Figure 3: Tripod mechanism in action. The celestial body shows relative motion due to earth's rotation.

As can be seen in figure 1, the camera is positioned at the center of the platform such that its viewing vector is parallel to the normal of the platform. This leads to equal distribution of load on all three legs. This configuration involves rotation and linear displacement of the camera when the mechanism is actuated. Since the observed object is at infinity, therefore the displacement along the viewing vector has no effect. The mechanism is actuated by the modified leg which contains the segment made of active hydrogel material PNiPAAm. Since, it is a thermally controlled actuator, therefore heat source, power source, and micro-

controllers are also fitted in the modified leg. The magnified cross-section view shows the schematic design and components of the actuator segment. The actuator is a cylindrical geometry of active hydrogel sealed inside a thin membrane (e.g. polyethylene bag) to render it as a thermodynamic closed system. The shape and volume of the membrane is such, that it provides no resistance during the swelling of the actuator and holds the excess water during the deswollen state, see figure 4. Two commercially available disk shaped mini-heaters (for instance, heaters used in aquariums, see figure 5) are attached on both ends of the actuator such that they are also inside the membrane and in contact with the gel.

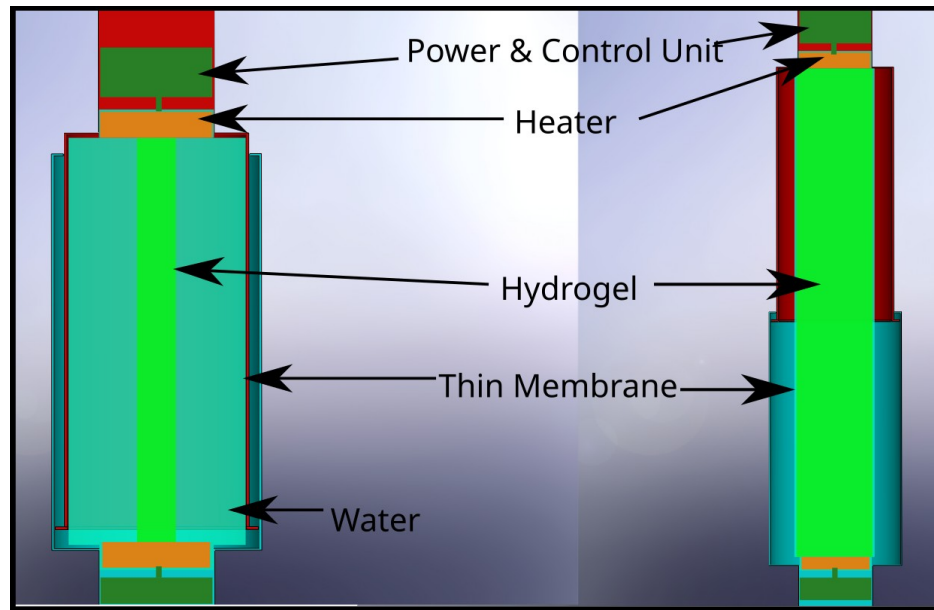


Figure 4: Actuator in deswollen state (left) and swollen state (right).

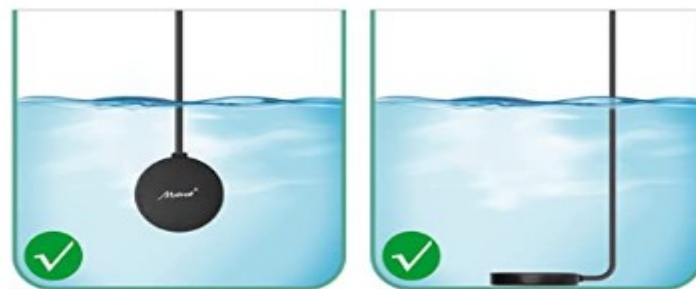


Figure 5: Commercial aquarium heater. Image source (Mylivell 2021).

The power source and micro-controllers are also placed inside the modified leg. The actuation is controlled by programming or giving input to the controller based on requirements of the user. The entire actuator assembly is fixed at both ends such that it

does not displace during operation. The assembly is encased by an outer shell made of light-weight and rigid material. The dimensions of the shell are determined to accommodate the expelled water during shrinking. The casing is an assembly of two halves to enable deformation and also to allow air inflow/outflow to compensate for the void created during the intake of water by the gel in swollen state.

Having addressed the various scientific aspects of tripod design, it is the right occasion to discuss about the engineering aspects of design. The thesis work is centered around determining the loads that the actuator will bear and the corresponding design parameters of the actuator to produce the required strain under those loads without failing. Figure 6, shows the schematics of load application on the actuator. This paves the path to develop a finite element model with appropriate loading and boundary conditions.

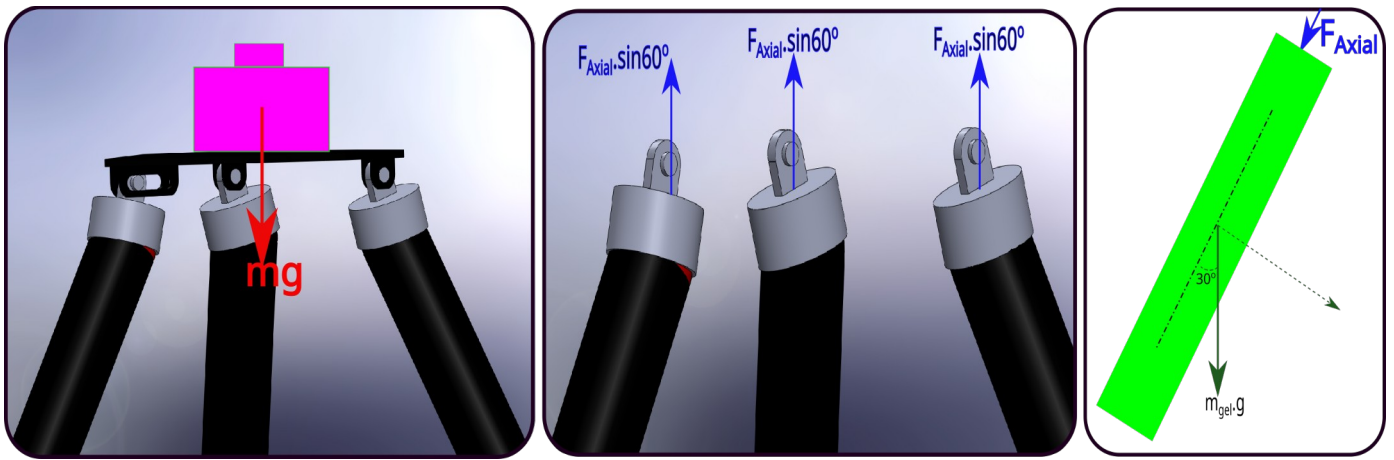


Figure 6: Acting forces on tripod legs.

The thesis is structured in the following way. Chapter 2. introduces the hydrogel materials and their properties. The theory, mechanism and modelling of their swelling process is also discussed. The analytical model NETEM used to model the actuator for the tripod is also presented in this chapter. The application of this model, together with other constraints and mechanical phenomena, leads to analytical determination of the geometry parameters for the actuator, which serves as the starting design point for the FEM model. Then, the simulation modelling and setup on ABAQUS is presented. Chapter 3. is all about simulation results and its discussion. Here, important inferences are drawn out. Drawbacks and shortcomings of the tripod and actuator are also pointed out. Finally, chapter 4. contains the conclusions and scope for future work.

2. Hydrogel Application in Engineering: The What and The How

In the current chapter, fundamentals about hydrogels will be given. Particularly, their properties and some basic chemical background will be discussed, to lay the base for thesis work. The swelling properties will be presented and a model to explain the mechanism of swelling is also discussed. The analytical model to simulate hydrogel structures is explained, which is followed by the designing of the tripod actuator. The FEM model for the simulation is also presented in this chapter.

2.1 Introduction to hydrogels

As described in Gerlach (2010), hydrogels are a special kind of polymer gels which are hydrophilic in nature and characterized by a large number of cross-linked monomers. These two attributes enables the hydrogels to absorb large quantities of water without getting dissolved. Beside these two basic properties, hydrogels have remarkable properties of softness and stimuli-responsiveness as discussed in Tanaka (1981) and Shibayama (1993). The hydrophilicity of these gels can be attributed to the hydrophilic functional groups that are attached to the main polymer chain. The polymer chain acts as a matrix that holds the water inside the gel, and the water inside the gel acts as a medium for some solute molecules to diffuse. The connections between the network chains render the gel as one big polymer molecule on a macroscopic scale. Since gel is an intermediate state between liquid and solid, it exhibits properties not found in either pure liquid or pure solid. Due to their quasi-liquid quasi-solid state, their mechanical properties are characterized by an elastic modulus, with a noticeable plateau region, and a viscous modulus whose value is significantly low in the plateau region. The hydrogel structure and properties, like swelling and elasticity, are strongly dependent on the external conditions under which they are synthesized, for example initial degree of dilution of monomer, temperature, cross-linker concentration, etc.

As mentioned in the previous paragraph, hydrogels respond with an isotropic volume change when exposed to an external stimulus, like light, temperature, pH change, biochemicals, etc, shown in figure 7. Hydrogels can be mono-sensitive i.e. they respond to a single stimulus. In reality, they are more often multi-sensitive i.e. more than one stimuli can elicit a response from the hydrogel (Ehrenhofer 2020a). When the effect of one stimulus dominates the others, the hydrogel can be approximated as mono-sensitive. Another solution is to operate the hydrogel with the preferred stimulus while keeping the others at a fixed state.

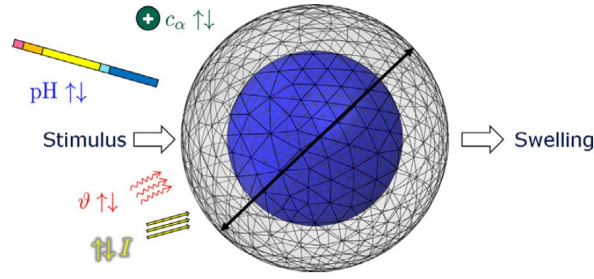


Figure 7: Stimuli-responsive hydrogel material. Image taken from Ehrenhofer (2018).

The degree of swelling is quantitatively defined by one of the two measures, mass swelling ratio or volume/diameter swelling ratio. The mass swelling ratio is the ratio of mass of swollen hydrogel in actual state to the mass of dry hydrogel at reference state, $Q = m_{act}/m_{dry}$. Analogously, the volume swelling ratio is the quotient of gel volume at actual state and gel volume at reference state, $q = V_{act}/V_{ref}$. The mass swelling ratio, due to its convenient measure-ability, is more prevalent than the volume/diameter volume swelling ratio which requires optical or manual methods for measurements. However, under some assumptions, these measures are inter-convertible. The swelling measure at a given state, together with the stimulus value at that state gives the characteristic swelling curve for that hydrogel material. Figure 8, shows four typical swelling behaviour curves under which most of the hydrogels can be classified.

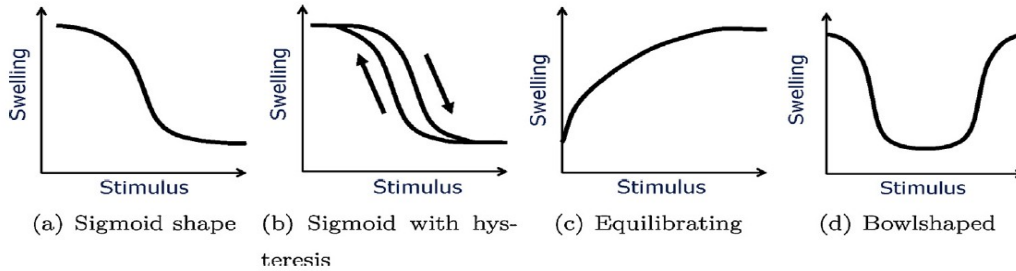


Figure 8: Typical characteristic swelling curves of hydrogels. Image taken from Ehrenhofer (2018).

In the present work, the chosen hydrogel material is poly(N-isopropylacrylamide), PNiPAAm. It is a thermo-sensitive hydrogel with LCST (lower critical solution temperature) swelling behaviour. The term LCST conveys the existence of a critical temperature below which the hydrogel is always in the swollen state. For PNiPAAm, the LCST is about 32.9°C. PNiPAAm consists of hydrophobic (parent chain and isopropyl group) and hydrophilic (amide group) parts. At temperatures below LCST, the amide-water bonding dominates, resulting in a swollen hydrogel. The hydrophobic interaction overshadows at temperatures

above LCST, expelling the water out of the gel. Figure 9 shows an experimental data plot for PNiPAAm.

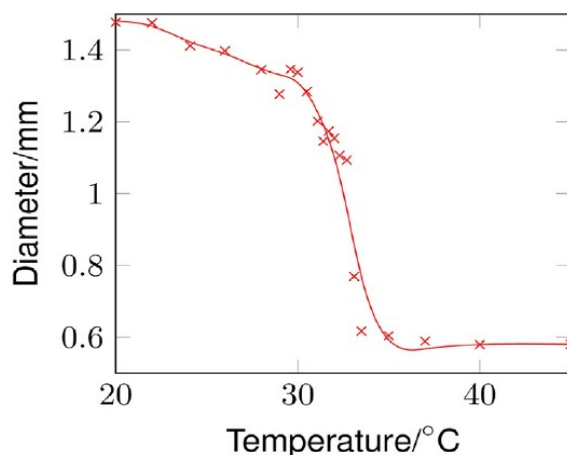


Figure 9: Swelling curve of PNiPAAm hydrogel obtained from experimental data. Image taken from Ehrenhofer (2018).

2.2 Basic chemistry of swelling

The swelling of hydrogels is essentially a chemical process, wherein the solvent is absorbed from a liquid or gaseous source by the cross-linked polymer. This results in a phase change from dry polymer to a polymeric gel. Akin to every chemical process, there are two aspects associated with hydrogel swelling viz. thermodynamics (the study of process feasibility, properties, extent of process, and equilibrium-state) and kinetics (the study of rate and path of the process). The following sub-sections give an overview of these two aspects for swelling, the comprehensive theory of which can be found in Gerlach (2010).

2.2.1 Thermodynamics of hydrogel swelling

When the dry polymer is placed in excess of liquid, the volume of the polymer starts to increase due to swelling and eventually an equilibrium state is reached. The equilibrium state or the extent of sorption can be manipulated by placing the gel in a solvent in gas phase at varying vapour pressures. Measuring the properties at different equilibrium states enable the determination of thermodynamic as well as material properties of the hydrogel.

Thermodynamics often deals with the chemical potential of a component, since a chemical process is an outcome of the difference between the potentials of participating components. Swelling (or shrinking) is a consequence of the difference between the chemical potentials of the solvent outside and inside of the polymer. The chemical potential of a component is a state function of temperature, pressure and number of

moles of each components, and is defined as the partial differential of Gibbs free energy of the system w.r.t its number of moles.

The deformation of the polymer network which ensures the swelling of hydrogel, alters the thermodynamic properties of the gel. Swelling is composed of two opposing processes taking place simultaneously, namely:

- Increase in entropy of the network-solvent system as the solvent molecules enter the polymer network.
- Decrease in entropy of the network chains due to their elongation/stretching.

When solvent molecules are introduced inside the network, they scatter throughout the polymer structure due to Brownian motion. This resembles a typical dissolution process wherein the solute particles disperse through the solvent. The upshot of this dispersion is the increase in entropy of the solvent-network system. Contrary to this, the volume increase of the polymer network leads to an elastic restoring response from the polymer chains. This induces a decrease in the entropy of the polymer chain. At the swelling equilibrium, both of these contra-processes equalize.

A theoretical model to determine the swelling equilibrium condition was proposed by Flory and Rehner (Flory 1944), (Flory & Rehner 1943a) and (Flory & Rehner 1943b) called Flory-Rehner Theory. According to this theory, the change in free enthalpy during swelling can be separated into two contributions viz. the free enthalpy of mixing solvent and polymer, and the free enthalpy of elastic deformation. The basic relation between Gibbs free energy and chemical potential of a component means that the partial differential of Gibbs free enthalpy w.r.t number of moles of a component gives the chemical potential difference for that component. Here, the chemical potential difference corresponds to the solvent, inside and outside of the polymer network. Hence, the sum of chemical potential difference for mixing and chemical potential difference for elastic deformation gives the total difference in chemical potential of solvent. The mixing contribution is determined by Flory-Huggins (FH) equation while the Rubber Elasticity Theory (RET) forms the basis for calculating the elasticity contribution.

Besides these two prevalent contributions, various intermolecular forces like Van der Waals forces, hydrogen bonding, hydrophilic and electrostatic interactions, play a significant role during various phase transitions in the gel. The influence of these forces are accommodated as additional terms to free enthalpy.

Moreover, the chemical potential difference can be used to derive a more perceptible quantity namely, the osmotic pressure. In Flory (1953), the analogy between swelling equilibrium and osmotic equilibrium has been drawn by Flory. A new quantity called swelling pressure was calculated as a difference between the osmotic pressure and the

elastic restoring force of the polymer chains in the swollen state. These calculations obviate the fact that a swelling or shrinking hydrogel produces a force. It is this generated force which gives hydrogels the ability to be used as actuators. At equilibrium, the swelling forces become equal to the restoring forces. This only corroborates the statement that the difference in chemical potentials of the solvent, inside and outside of the gel, is zero at equilibrium.

2.2.2 Kinetics of hydrogel swelling

Swelling kinetics determine the time for swelling or deswelling processes like absorbing or delivering a swelling agent or dissolved substance in the solvent. It also helps to determine the characteristic response time of a hydrogel when stimulated with changes in its environmental conditions. The application of hydrogels as sensors or actuators is based on the change in their degree of swelling, which is in-turn controlled by applying a physical stimulus, like changing the surrounding temperature. It becomes imperative to determine their response time in order to get desired outputs. Therefore, it is paramount to study the swelling kinetics and ascertain the factors that could be exploited to influence it.

Swelling, in general, is a process where diffusion of different components take place. There are two approaches to understand and study the swelling kinetics. One way is to consider the hydrogel as a discontinuous medium and account for the processes at microscopic level. During swelling, the solvent diffuses into the polymer while the polymer chains alter their conformation, since they expand. Alfrey Jr (1966) and George (2004) proposed three models to describe the time-dependency of the degree of swelling, based on the relation between the rate of solvent diffusion and rate of relaxation of polymer chain. The three models are described below.

- Case 1 or Fickian diffusion: The rate of diffusion is significantly lower than that of relaxation of polymer chains. The change of the degree of swelling is thereby governed by the diffusion of the swelling agent. The mass increase (degree of swelling) is proportional to the square root of the diffusion time.
- Case 2 diffusion: The rate of diffusion is higher than that of relaxation of polymer chains. The mass increase of the hydrogel is proportional to the time.
- Case 3 or anomalous diffusion: Both the rates are almost similar. The exponent of the time in the proportionality relation between degree of swelling and diffusion time lies between 0.5 and 1, i.e. case 3 is intermediate between case 1 and case 2.

The observed characteristics of a polymer, like the microscopic processes during swelling, the form of diffusion profile, the location and concentration of the solvent, the variation of mechanical properties etc, determines the type of diffusion (Case 1,2 or 3) that takes place in the polymer.

The second much easier approach to monitor the swelling kinetics, is to track the change in macroscopic properties like size or weight (degree of swelling) with time. The swelling kinetics is expressed as a collective diffusion process in the theory for polymeric gel dynamics presented in Tanaka (1973). The theory was predicated on the realization that polymer chains are connected by chemical bonds and hence, a gel should be treated as a continuum. Moreover, the polymer acts as a network of springs due to their elasticity.

In short, Tanaka et al. derived an equation of motion from the generic transport equation from which the source term and convective term were truncated. This resulted in a diffusion equation which determined the displacement of a point on the network from its average position. The diffusion coefficient of this equation depends on gel properties, namely friction coefficient of network-solvent, the bulk modulus and the shear modulus. For a swollen polymer gel, all these three properties depend on the degree of swelling. Consequently, the diffusion coefficient also has a proportionality relation to the degree of swelling. This diffusion coefficient is termed as cooperative diffusion coefficient and accounts for the collective diffusion that takes place during the swelling or deswelling process.

The cooperative diffusion coefficient D_{coop} can be gauged directly by experimental methods, e.g DLS (Dynamic Light Scattering) leverage the fact that due to random thermal motion of the polymer chains, there exists spatial and thermal inhomogeneities in polymer concentration. The scattering of an incident light due to these inhomogeneities is studied, to derive a correlation function and diffusion coefficients. However, due to the strong influence of inhomogeneities on scattering properties, it is quite difficult to determine D_{coop} by DLS (Shibayama 2002).

Since there exists a proportionality relation between D_{coop} and degree of swelling (as mentioned in two paragraphs above), a simpler way to calculate D_{coop} is by measuring the degree of swelling (change in size or weight) of a hydrogel sample of defined geometry as a function of time. This is exemplified in Tanaka (1979) and Li (1990), where the change of radius r of a spherical gel w.r.t time due to swelling is calculated as:

$$\frac{r(t=\infty) - r(t)}{r(t=\infty) - r(t=0)} = \frac{\Delta r(t)}{\Delta r_0} = \frac{6}{\pi^2} \sum_{n=1}^{\infty} n^{-2} \exp\left(-n^2 \frac{t}{\tau}\right) \quad (2.1)$$

For a long swelling process ($\frac{t}{\tau} > 0.25$), the above equation simplifies as:

$$\ln \frac{\Delta r(t)}{\Delta r_0} \Big|_{t \rightarrow \infty} = \ln \frac{6}{\pi^2} - \frac{t}{\tau} \quad (2.2)$$

The cooperative diffusion coefficient is calculated as:

$$D_{coop} = \frac{r_{\infty}^2}{\pi^2 \tau} \quad (2.3)$$

Here, τ is the characteristic swelling time of the material and r is the characteristic length of the geometry. $t=\infty$ denotes equilibrium state and $t=0$ the initial state.

However, these equations are valid for spherically symmetrical geometries. In real case scenarios, most common used geometries are cylinder (as is the case in this thesis work) or strips. The inherent simplification of spherical geometries does not apply on other geometries. Therefore, modifications are done in the equations to account for shear modulus and anisotropy in swelling for different geometries. For this thesis work, we are interested in cylinders. Therefore, a correction term f to account for cylindrical geometry of arbitrary aspect ratio (AR) is given in Krause (2016) and defined as:

$$AR_{worm} (h/d) > 1, f_{h>d} = \frac{(1 + 2 AR_{worm})}{3 AR_{worm}} \quad (2.4)$$

$$AR_{cylinder} (d/h) > 1, f_{d>h} = \frac{(AR_{cylinder} + 2)}{3 AR_{cylinder}} \quad (2.5)$$

where, d and h are the diameter and height of the cylinder, respectively. Then, the final D_{exp} , that is applicable in real scenario, is calculated as:

$$D_{exp} = f D_{coop} \quad (2.6)$$

Also, the radius of the sphere is taken as the characteristic length in the original equations. In the case of cylinders, the characteristic length is half of the cylinder height (for disk-like cylinders) and radius of the cylinder (for worm-like cylinders).

2.3 Swelling Model

To understand the working of internal mechanism of the hydrogel, a two-step model for volume-phase transition, is presented and elucidated in Gerlach (2010). In the first step, the applied stimulus infuses into the gel. The rate of the first-step is determined by the type of stimulus applied, e.g. heat-transfer rate for temperature change (thermo-sensitive gels) or mass-flow rate for composition change (chemo-sensitive gels). If the applied stimulus corresponds to the condition for a volume phase transition, then swelling/deswelling initiates. In the second step, a change in the degree of swelling occurs in response to the applied stimulus. The rate of this step is governed by the cooperative diffusion coefficient D_{coop} , as discussed in section 2.2.2. Figure 10 visualizes and summarizes the two-step model of swelling.

In the current thesis work, a thermo-sensitive gel PNiPAAm is considered here to explain the model and its rational. It is an established fact that the mechanical properties of the hydrogel depends on the degree of swelling (Seuss 2016). The volume phase transition and the applied temperature change about that point can be done as an isobaric or as an isochoric process. For PNiPAAm, the volume phase transition occurs at around 33°C and a sudden increase in the bulk modulus is recorded at this temperature during heating.

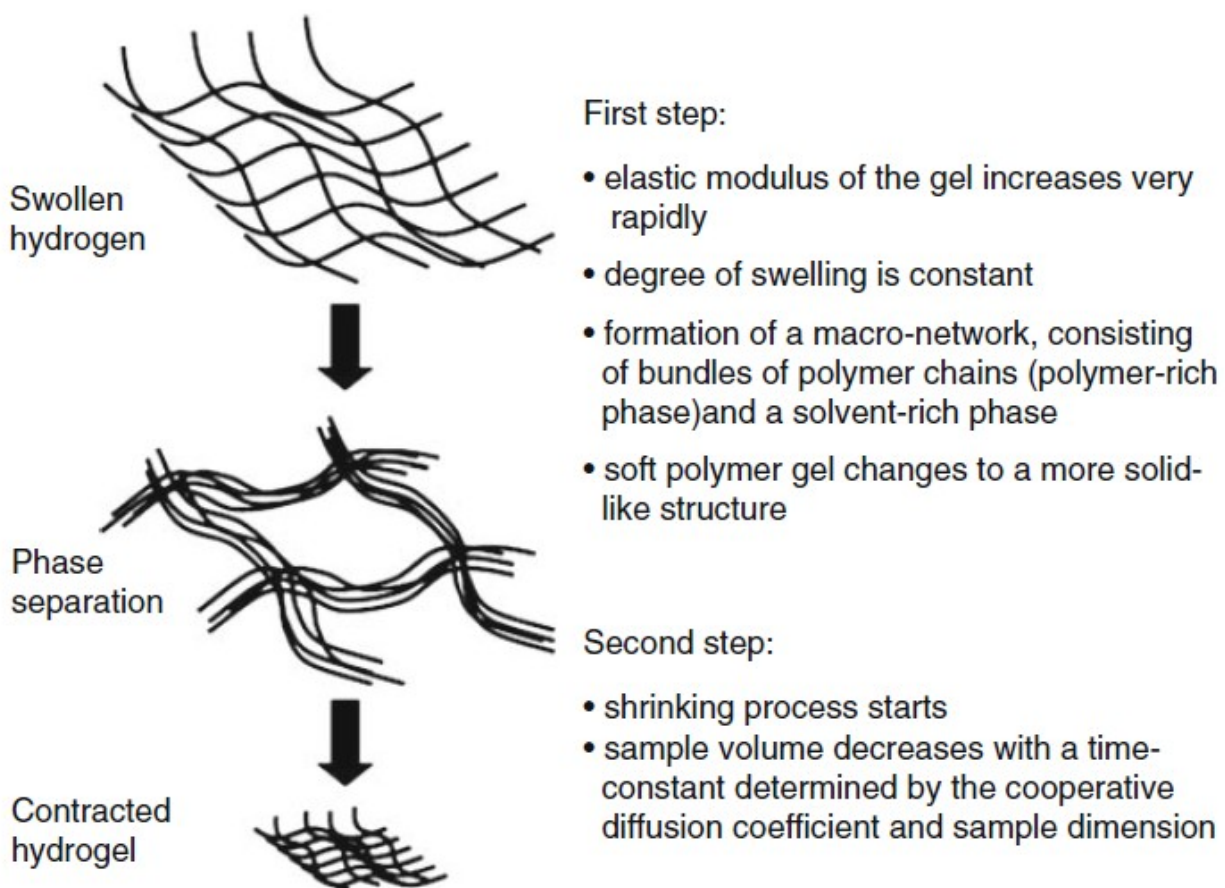


Figure 10: Two-step model of swelling mechanism. Image taken from Gerlach (2010).

If the process is conducted isobarically, this sharp increase in the mechanical properties can be attributed to the volume change (shrinking) that occurs at the transition temperature. But if the heating is done as an isochoric process, the volume is unchanged. The older theories predict mechanical properties to remain almost same, due to constant polymer concentration. However, experimental data again show an abrupt increase in the elastic modulus.

Shibayama (1994) delineates phase transition for a polymer solution as segregation of the solution into a polymer-deficient phase and a polymer-rich phase. The polymer chains form bond and forms coil globules. The two-step model uses this as an analogy to explain

the enhanced mechanical properties during isochoric shrinking. While such macroscopic transition does not occur in gels, the network chains can still form a macro-network that consists of bundled chains (see step 1 in figure 10). These polymer-rich bundles are surrounded by the polymer-deficient phase, resulting an increase in the elasticity of the material at the same (high) degree of swelling.

2.4 Methods of reducing the response time of hydrogels

As discussed in section 2.3, the rate of change of degree of swelling (swelling/ deswelling) and the response time τ during the volume phase transition of the hydrogel hinge on the value of cooperative diffusion coefficient D_{coop} and the square of its characteristic length. Following is the relation:

$$\tau \sim \frac{length^2}{D_{coop}} \quad (2.7)$$

Typical values of D_{coop} are in the order of $10^{-7} \text{cm}^2/\text{s}$. This results in a very slow response which is impractical for real application. One of the ways to effectively reduce the response time is by reducing the characteristic length of the gel geometry. Enlisted are various techniques¹ to achieve the desired performance:

- Synthesizing porous or sponge-like gels (Dong 1990), (Jian 2022) - By making the gel porous, the characteristic dimension is significantly reduced and also the surface area in contact with the solvent increases. The response of porous gels is very fast in contrast to the non-porous gels. However, the mechanical stability and properties are badly affected.
- Introducing hydrophobic clusters in the gel. This increases the cross-linking density and forms additional junction points, effectively reducing the size of polymer chain globules, inside which the interaction occurs during diffusion.
- Manufacturing gel particles in the micro-meter range (micro-gels) using techniques like inverse emulsion polymerization.
- Carrying-out cross-linking of polymers in the presence of an inert substance to form macro-porous hydrogels.
- Cross-linking spin-coated thin films of polymer on a support under UV radiation or high energy radiation (electron-beam, etc).

¹ All relevant citations can be found in Gerlach (2010)

- Forming gels with dangling chains. Since one side of a dangling chain is free, therefore they easily expand or collapse when stimulated. These dangling chains are attached on the gel particles.

2.5 Normalization of hydrogel swelling behaviour

As discussed in section 2.1, hydrogels have the capability to respond by either swelling or shrinking when stimulated by a change in their external environment. There are various types of stimuli such as, temperature, light, ionic concentration, pH value, biochemicals, etc. It is this property of hydrogels that enables them to be used as sensors or actuators. However, it is a specific swelling behaviour of the hydrogel which renders them suitable to be used either as a sensor or as an actuator. During the design phase of a product, based on the requirements, a material is shortlisted from a catalogue or database of materials. Due to the limited application and obliviousness of the industry to the capabilities of hydrogels, not much work is done in the direction of database compilation for hydrogels. To exacerbate this situation of material selection, different measures for swelling are reported in the literature, which makes material comparison impracticable.

Ehrenhofer (2018) and Ehrenhofer (2017) present an approach to generalize the swelling behaviour of hydrogels. This process of normalizing the stimulus and response data of different hydrogels, provides a way to compare and determine the suitability of a hydrogel for sensoric or actuatoric application. Figure 11, depicts the process-flow for normalization.

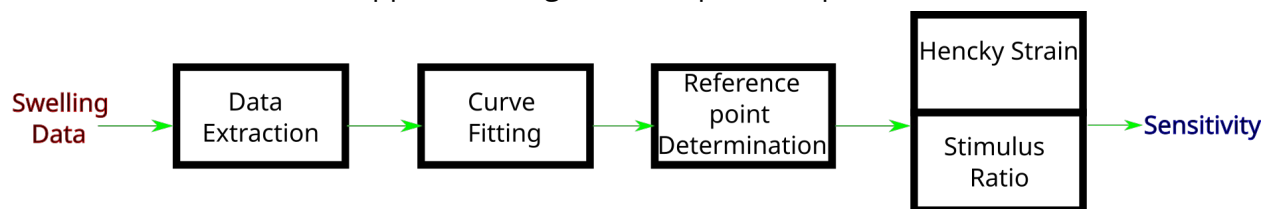


Figure 11: Procedure for Normalization of swelling behaviour. Image adopted from Ehrenhofer (2017).

First, the swelling data is acquired either by conducting experiments or from the literature. When literature is used, the data needs to be extracted with the help of a digitizer tool since most of the time comprehensive machine readable data is not provided by the authors. Hence the process begins with Data Extraction, wherein the data can be masses/mass-swelling degrees or volumes/volume-degrees against the stimulus values.

Since swelling is a slow process and also recording swelling data is a laborious task, therefore limited data points are measured in an experiments. Curve Fitting is performed to estimate a continuous swelling-stimulus function using the available discrete data points. For a given hydrogel material, the function can be predicted based on its swelling mechanism. For instance, the swelling curve for thermo-sensitive materials (like PNiPAAm)

is a sigmoid function. Figure 12 contrasts three fitting functions (namely, piece-wise Cubic Hermite Inter-Polation splines (PCHIP) and two sigmoid functions based on an error function and a tanh() function) used for the swelling data of PNiPAAm by the authors.

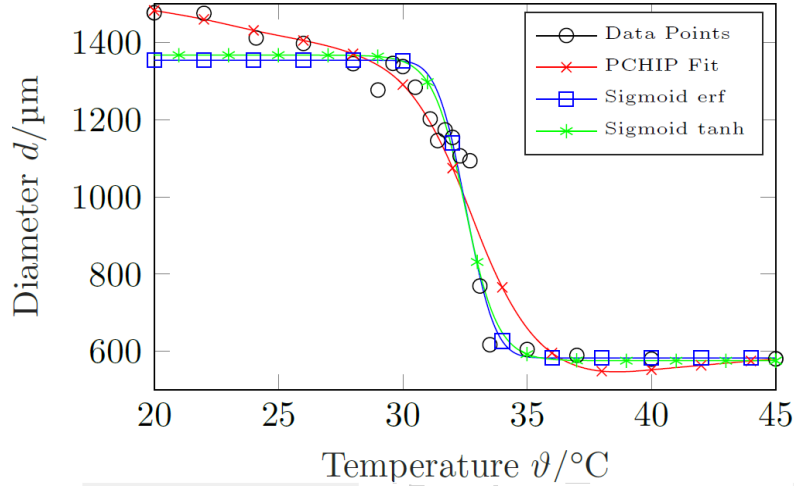


Figure 12: Comparison of different curve-fitting methods for data points. Image taken from Ehrenhofer (2017).

Once the swelling curve is obtained, the next step is to define a reference state or reference point, which is needed to normalize the swelling data. In principle, any arbitrary point can be taken as the reference point. When free (no external bearings or loads) isotropic swelling is conducted for thermo-sensitive hydrogel, the inflexion point of its sigmoid curve is taken as the reference point, in congruence with the definition of sensitivity parameter (see below). However, when mechanical loads are also applied during swelling, the stress-free state (which corresponds to the external conditions under which the gel was synthesized) is taken as the reference point. In this thesis work, the reference state is characterized by the pair of temperature T_{ref} and cylinder height H_{ref} .

With the determination of the reference state values, the swelling-stimulus data is normalized. The parameter used to describe the normalized swelling is the Hencky strain or logarithmic strain. The general expression of Hencky strain is as follows:

$$\varepsilon_{KL}^H = \frac{1}{2} \ln(F_{kK} F_{kL}) \quad (2.8)$$

Here, F_{kK} is the deformation gradient² between actual state and reference state. The quantity inside the ln-function is the right Cauchy-Green deformation tensor. The choice of Hencky strain over the simple technical strain is explained by the fact that hydrogels show large finite deformations which cannot be described by linear equations. Also, the

² For comprehensive reading refer Singularity (2020)

summation of mechanical strain and swelling strain (as needed in the thermo-mechanical material law) can be easily done as a multiplicative operation inside the ln-function. For this thesis work, the strain expression reduces to:

$$\varepsilon_{KL}^H = \ln\left(\frac{H_{act}}{H_{ref}}\right) \quad (2.9)$$

where H_{act} is the height of the cylinder in actual state and H_{ref} is the height in reference state. The parameter used to represent the normalized stimulus values in a way that it embodies any arbitrary stimulus, is the Stimulus ratio and is formulated as:

$$F^{Stimulus} = \frac{S}{S_{ref}} \quad (2.10)$$

where S is the stimulus value at actual state and S_{ref} is its value at reference state. In this thesis work, temperature T in the Celsius scale is the applied stimulus. The temperature can be taken in Kelvin scale also. The strain produced will be same for both the scales, as the value of expansion coefficient also changes according to the scale used.

Finally in the last step, the sensitivity of the hydrogel material is derived from the normalized strain and stimulus values. In analogy to signal processing, the term sensitivity is defined as the ratio of output parameter to input parameter. For hydrogels, it is formulated as:

$$Sensitivity = \frac{Swelling\ Parameter}{Stimulus\ Parameter} \quad (2.11)$$

Thus, a material that produces large swelling for a small stimulus is labelled as sensitive and is suited for sensoric applications. The inverse case of sensitive materials which shows high resistance to applied stimulus are suited for actuatoric applications. Figure 13 visualizes the intuition behind sensitivity with an example swelling-stimulus sigmoid curve.

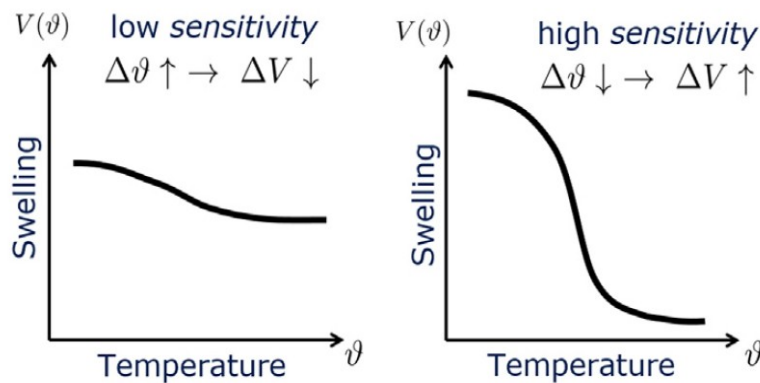


Figure 13: (Left) Suitable for actuatoric application, (Right) Suitable for sensoric application.
Image taken from Ehrenhofer (2018).

Mathematically, the sensitivity is defined as the slope of the $\varepsilon^H - F^{Stimulus}$ curve at the reference point (the inflexion point for sigmoid curve). With the sensitivity parameter, it is possible to contrast and assess different hydrogel materials for a given application. Figure 14 is the outcome of normalization of swelling behaviour of six different hydrogels which respond to different types of stimuli (Ehrenhofer 2018).

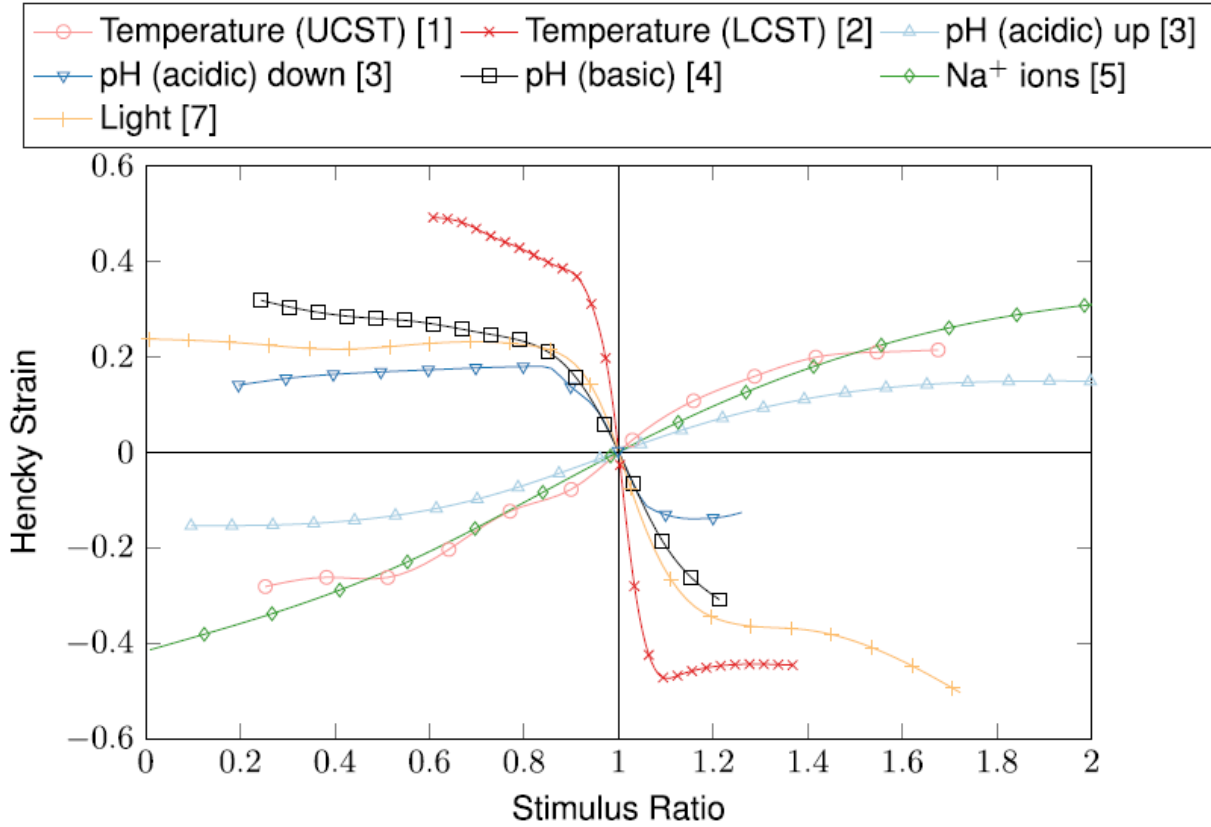


Figure 14: Normalized swelling curves of six different hydrogel materials. Image taken from Ehrenhofer (2018).

2.6 Normalized Extended Temperature Expansion Model

For the current work, the Normalized Extended Temperature Expansion Model (NETEM) is used to do the analytical modelling of the actuator and to derive the equations for numerical implementation in the solver. Contrary to the model given in Mazaheri (2019), the NETEM is a purely macroscopic model and does not take into account the actual swelling processes that take place inside the gel. The parameters for the material are gained from experimental data. Fundamentally, it is based on the analogy between thermal expansion and free isotropic swelling, hence the name Temperature Expansion Model

(TEM). Similar to the equation of thermal expansion, the expansion coefficient in TEM, as described in Ehrenhofer (2016), was defined using linear expansion (technical strain ε). Hence, TEM was essentially a linear model applicable for small deformations. The model was then generalized in Ehrenhofer (2017) to accommodate finite deformation by deriving a nonlinear expansion coefficient, and the model then became extended TEM (ETEM). The model was further generalized to incorporate arbitrary type of stimuli, when the swelling-stimulus behaviour was normalized in Ehrenhofer (2018), as shown in the previous section. The model in this form was called Normalized Extended Temperature Expansion Model. Figure 15 shows the evolution of the model.

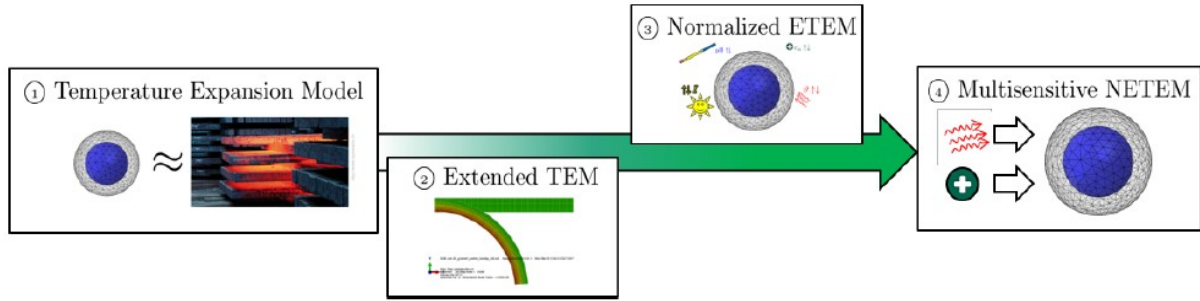


Figure 15: Evolution of NETEM model over the years. Image taken from Ehrenhofer (2020).

Ehrenhofer (2018) describes a method to implement the model on FEM tools like *ABAQUS*, so as to simulate swelling/deswelling of arbitrary structures and mechanisms made of hydrogel materials. This model is used in this thesis work to determine the dimensions of the cylindrical actuator segment of the tripod leg required to produce the desired strain and consequently, the desired rotation of the camera. The system of equations defining this thermo-mechanical model is as follows:

$$\sigma_{kl,k} + f_l = 0; \sigma_{kl} = \sigma_{lk} \quad (\text{Balance Laws}) \quad (2.12)$$

$$\varepsilon_{kl}^H = \frac{1}{2} \ln(B_{kl}) \quad (\text{Kinematics}) \quad (2.13)$$

$$\sigma_{kl} = E_{klmn} \left(\varepsilon_{mn}^H - \beta (F^{\text{Stimulus}}) \delta_{mn} \Delta F^{\text{Stimulus}} \right) \quad (\text{Constitutive Equation}) \quad (2.14)$$

Here, ε_{kl}^H is the total strain (Hencky strain, see section 2.5), σ_{kl} is the Cauchy stress tensor, $\sigma_{kl,k}$ is the derivative of the stress tensor w.r.t x_k , f_l are the volume loads, E_{klmn} is the elasticity tensor. In the Saint-Venant-Kirchhoff-like elastic material law, the extra term is the strain due to swelling/ deswelling, which has an isotropic stimulus expansion coefficient β

(function of stimulus ratio, see section 2.5) and the difference in stimulus ratio $\Delta F^{Stimulus} = (F^{Stimulus} - 1)$. δ_{mn} is the Kronecker-delta.

2.7 Designing the Actuator for the Tripod

The current section is dedicated towards designing the actuator. The analytical calculations will yield the first design parameters, which are height and diameter of the hydrogel cylinder, which will act as guide for modelling the CAD and FEM models. Figure 16 is the flow-chart that portrays the steps for the designing process.

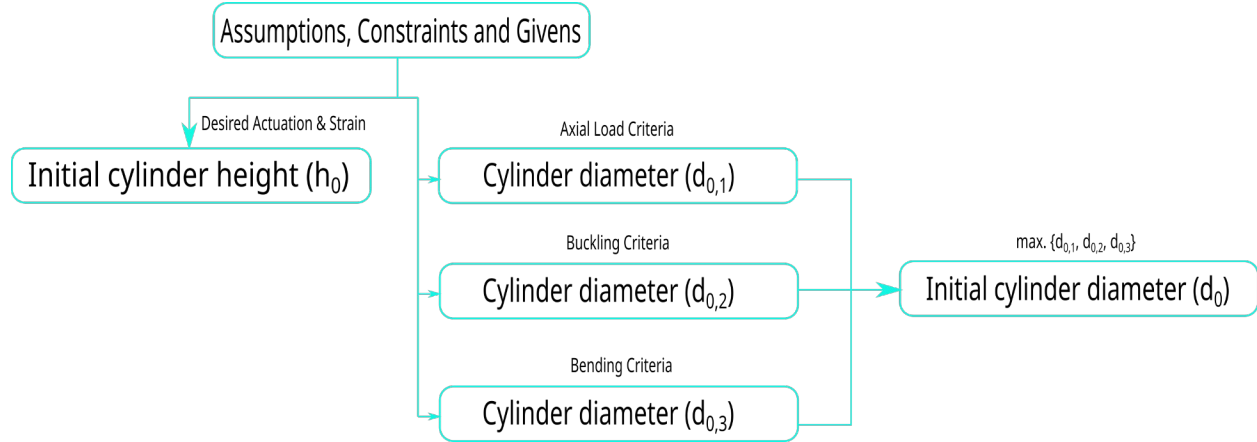


Figure 16: Flowchart of design process for this thesis.

2.7.1 Assumptions, Constraints and Givens

Just like any engineering design process, we start with gathering the “raw material” and setting-up the environment by specifying assumptions and constraints. Following is the list for the same:

- The material used to make the tripod platform and the legs is carbon fiber reinforced plastic. Legs are hollow cylinders. Due to its low weight in comparison to the camera, the load on the actuator due to leg-segment is neglected.
- Hydrogel material used is PNiPAAm. The material data for expansion is taken from the simulation model of Winkler (2020).
- Since its modulus of elasticity (E) is temperature dependent and determined experimentally, therefore a value of 80 kPa is estimated from literature for the initial state (Matzelle 2003).
- Water is taken as the solvent. ($\rho_{water} = 1000 \text{ kg/m}^3$)
- The density of hydrogel is assumed to be equal to that of water.

- The actuator is swollen in the initial state (at $t=0$).
- The camera considered in this thesis work is *CANON EOS Ra*³. The weight of this camera is 660 g. For this thesis, no additional lens or accessory is considered.
- The earth takes 24 hours for one rotation. The tripod is being designed to be able to take a long-exposure photo of upto 4 hours. As a limiting condition, the required rotation comes out to be 60 degrees (see figure 3).
- The corresponding required actuation length (l_f) (see section 3.5), which is the result of both mechanical load and thermal load, is 165 mm.

$$l_f = h_0 - h = 165 \text{ mm}$$

- For benchmarking and reference values, the commercial tripod mount *EQ3-2 + Synscan Upgrade Kit*⁴ is selected. The mount has a resolution of 0.283217 arcsecs (= 0.000078671°). This will serve as the reference tolerable error in actuation $\delta\theta$ in this thesis work.
- There is a constraint between the actuation length l and the angle of camera rotation θ with the vertical axis. The Law of Sines gives the constraint equation:

$$\frac{\sin \theta}{\sin(120 - \theta)} = \frac{l}{l_f} \quad (2.15)$$

- To make the effect of angle change due to mechanical load negligible in comparison to the effect caused by the hydrogel swelling, following strain constraint is assumed:

$$\varepsilon_{mech}^H = \frac{1}{1000} \varepsilon_{th}^H$$

- Temperature at initial state (T_0) is assumed to be at 32°C.
- A temperature change (stimulus or thermal load, ΔT) of 4 K is applied.

2.7.2 Initial cylinder height

From the requirements stated above, it follows that

$$l_f = h_0 - h = 165 \text{ mm} \quad (2.16)$$

For the applied temperature change, the corresponding strain is:

³ <https://www.canon-europe.com/cameras/eos-ra/specifications/>

⁴ <http://eq-mod.sourceforge.net/prerequisites.html>

$$\varepsilon_{th}^H = \beta(F_{32-36}) \cdot (F_{32-36} - 1) \quad (2.17)$$

$$\varepsilon_{th}^H = -0.671$$

From the strain constraint defined in the previous section,

$$\varepsilon_{mech}^H = \frac{1}{1000} \varepsilon_{th}^H \quad (2.18)$$

$$\varepsilon_{mech}^H = -0.671 \times 10^{-3}$$

$$\varepsilon_{total}^H = \varepsilon_{mech}^H + \varepsilon_{th}^H = \ln\left(\frac{h}{h_0}\right) = -0.671671$$

$$\frac{h}{h_0} = 0.51085 \quad (2.19)$$

From equations (2.16) and (2.19), it follows that

$$h_0 = 337.32 \text{ mm}$$

$$h = 172.32 \text{ mm}$$

Thus, the initial height of the actuator is $h_0 = 337.32 \text{ mm}$.

2.7.3 Cylinder diameter: Axial compressive load criteria

The load due to the camera is equally distributed on all three legs, as shown in figure 6. The mass of the camera as specified in section 2.7.1 is 660 g. To take into account the safety factor of 1.5 and other small resistances, an acting load of 1 kg is taken for the calculations. The maximum load ($F_{max} = mg/3$) during the entire deswelling process, is experienced by the actuator when the platform is parallel (deswollen state) to the ground. As explained in section 2.3, the elasticity modulus of the gel increases when it deswells. Therefore, the actuator will be designed such that it can bear this maximum value even for the initial (swollen) state.

Now, the axial resistance developed in each leg is $F_{axial} = \frac{2 \cdot m \cdot g}{3 \cdot \sqrt{3}} = 3.8 \text{ N}$.

From equation (2.14), we have

$$\sigma_{axial} = E \cdot (\varepsilon_{total}^H - \varepsilon_{th}^H) \quad (2.20)$$

$$\frac{F_{axial}}{A} = E \cdot \varepsilon_{mech}^H$$

here A is the cross-section area of the actuator. The calculation of above equation yields

$$d_{0,1} = 300 \text{ mm}$$

The value of initial diameter due to this criteria comes out to be $d_{0,1} = 300 \text{ mm}$.

2.7.4 Cylinder diameter: Buckling criteria

The second phenomenon to consider, is buckling. Due to the design of the outer shell, the actuator is basically a fixed beam. For a given critical load (F_{cr}) of 3.8 N, the diameter is determined in the following:

$$(d_{0,2})^4 = \frac{64 \cdot L_{eff}^2 \cdot F_{cr}}{\pi^3 \cdot E} \quad (2.21)$$

$$\text{where, } L_{eff} = K L$$

Substituting $K = 0.5$ for a fixed beam (Alexander 2017) and h_0 as length L results in:

$$d_{0,2} = 40.866 \text{ mm}$$

The initial diameter due to buckling criteria comes out to be $d_{0,2} = 40.86 \text{ mm}$.

2.7.5 Cylinder diameter: Bending criteria

As discussed in the previous section, the actuator is essentially a fixed beam. Due to its own weight, it is prone to bending. This bending will have an effect on the total actuation length. Using the constraint equation (2.15) and $\delta\theta$, the tolerable error in actuation length δl is:

$$\delta l = \frac{l_f \sin \delta\theta}{\sin(120 - \delta\theta)} \quad (2.22)$$

$$\delta l = 0.00026 \text{ mm}$$

This leads to a resultant actuation length, $l_f - \delta l = l_{res} = 164.99 \text{ mm}$

From the bending deflection equation for a fixed beam under uniformly distributed load w , we obtain:

$$\delta_{max} = \frac{64 \cdot w \cdot L^4}{384 \cdot \pi \cdot E \cdot (d_{0,3})^4} \quad (2.23)$$

In lieu of data for deflection in camera tripods, the deflection tolerance was taken from civil engineering field of beam designing (Laing O'Rourke). As a safety measure, the allowed deflection is generally:

$$\delta_{allowed} = \frac{L}{250} \quad (2.24)$$

where L is the span length. The span length of the actuator to attain the desired precision is:

$$L = h + l_{res} = 337.319 \text{ mm}$$

Also, from figure 6, only the sine component of force acts as the load which gives:

$$w = \frac{\frac{(\pi \cdot h_0 \cdot (d_{0,3})^2)}{4} \cdot \rho_{water} \cdot g \cdot \sin 30^\circ}{h_0} \quad (2.25)$$

Substituting all the values in deflection equation yields:

$$d_{0,3} = 156.567 \text{ mm}$$

The bending criteria yields the initial diameter as $d_{0,3} = 156.57 \text{ mm}$.

2.7.6 Initial cylinder diameter

Following the flowchart in figure 16, the diameter of the actuator at initial (swollen) state comes out to be:

$$d_0 = 300 \text{ mm}$$

2.8 Finite Element Modelling and Simulation Setup

Using the dimensions determined analytically in the previous section, a finite element (FE) model of the hydrogel actuator is developed. The equations of the NETEM model are applied to simulate the actuation by the ABAQUS/Standard solver. Figure 17 shows the side-view of the 3D meshed model. The model is a cylinder of a diameter of 300 mm and a height of 337.32 mm made up of PNiPAAM material. The actuator is fixed at the right-side like a cantilever beam and the motion of the face-center on the left-side is constrained in the x and y directions. The face-center A on the left-side is tracked for displacement during the simulation. The model is discretized using quadratic hex-elements (cubes) of type C3D20RH. A coarse mesh with global element size of 20 mm (20x20x20) is used as the first case for the mesh convergence study. Non-linear kinematics were used to carry-out the simulations.

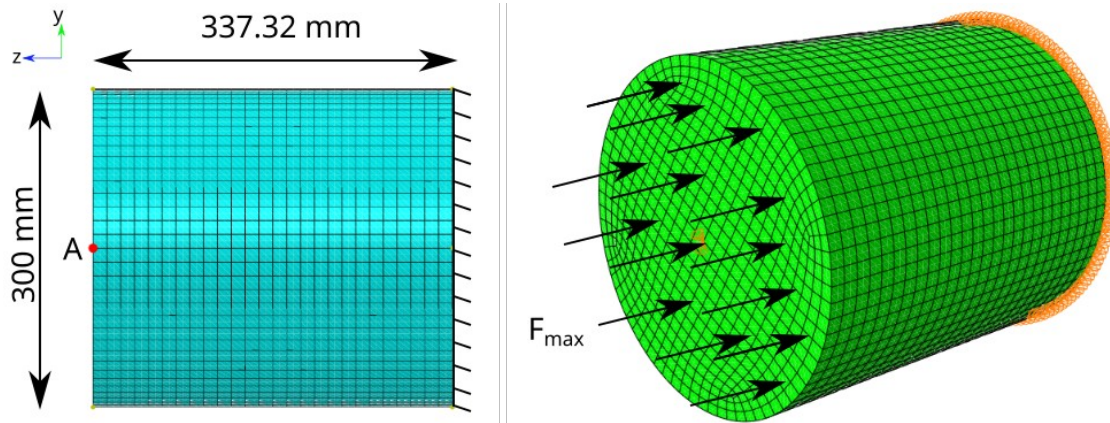


Figure 17: Simulation model setup.

The thermal stimulus is applied in the form of a linearly increasing temperature field from 32°C to 36°C, over the entire actuator. The axial load due to the camera weight is applied as a constant and uniform pressure load over the left face of the actuator. The simulation consists of two steps. The camera weight is applied on the left face in first-step and then the temperature of the system is increased in the second-step to induce the actuation. A total time of 20 s is simulated, which is equally distributed between both the steps.

3. Results and Discussion

This chapter presents the simulation results and discusses various observations made from the simulation study. The tripod design is further developed and modified to accommodate the actuator. The final tripod design is then explored both as a mechanism and as a structure. The actuator is also investigated against the given time-constraint and for its kinetic performance.

3.1 Simulation result and mesh convergence study

Figure 18 depicts the mesh converge study. All the simulations were carried-out using six Intel^(R) Xeon^(R) Skylake processor cores on a server computer. It can be seen that refining the mesh produces no change in the result, in other words the mesh was already converged for the mesh-element size of 20 mm.

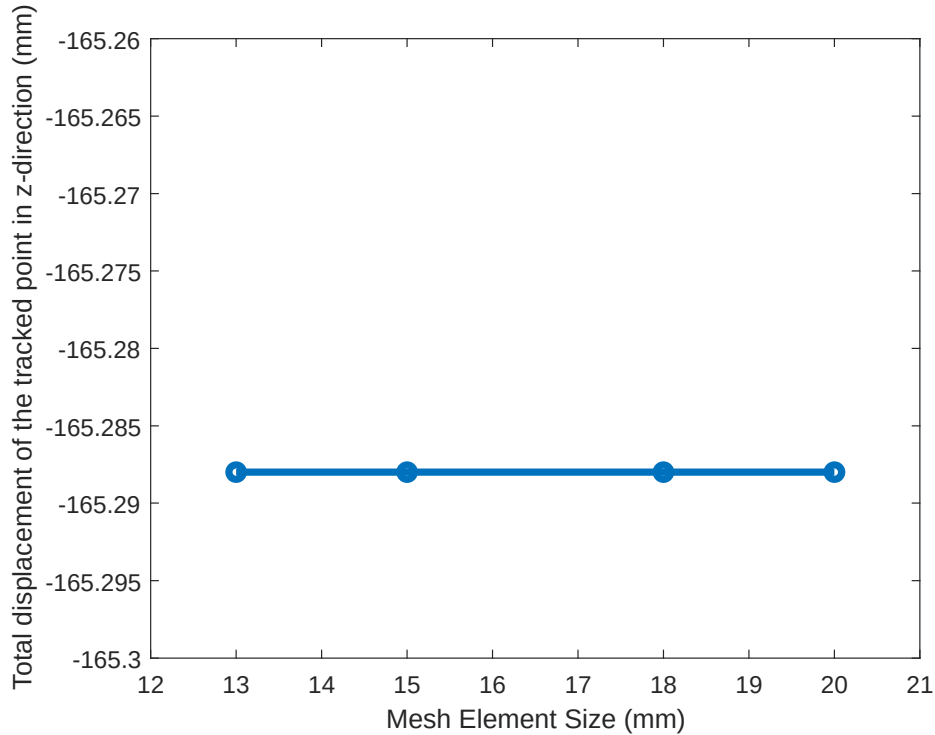


Figure 18: Mesh convergence study.

The displacement of the traced point in z-direction is shown in figure 19. In the first step, the camera weight produces a displacement of -0.2266 mm in z-direction. The corresponding Hencky strain due to the mechanical load is:

$$\epsilon_{mech}^H = -0.672 \times 10^{-3}$$

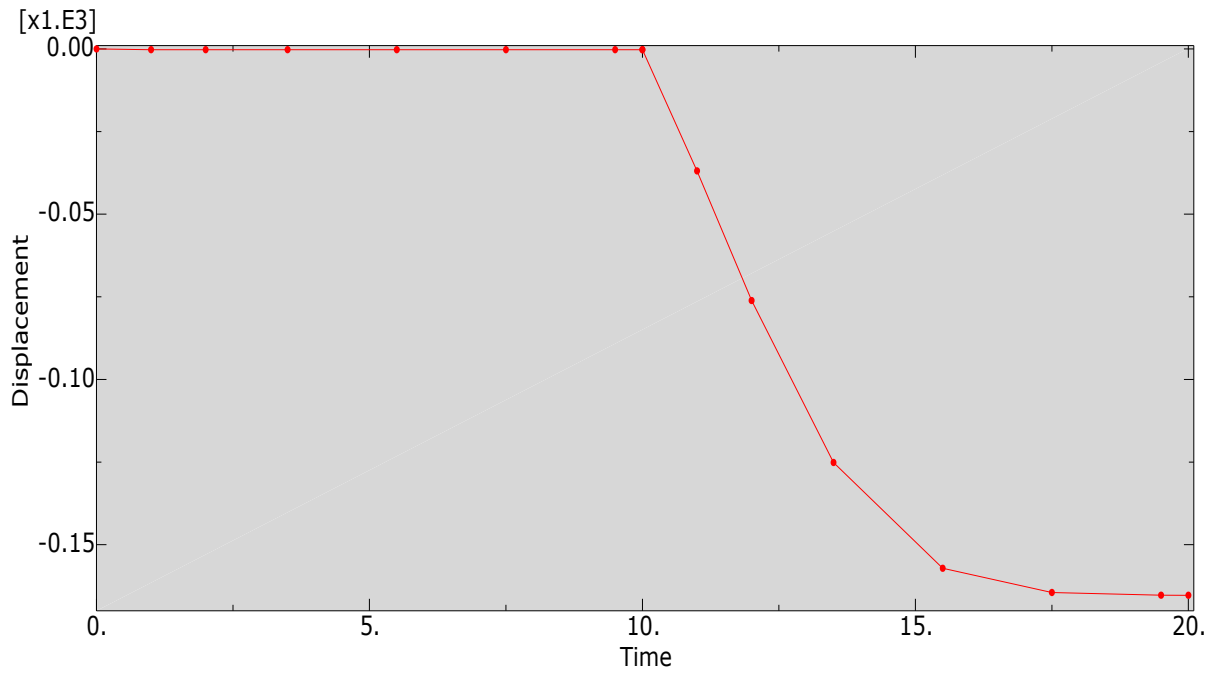


Figure 19: Displacement-time plot of the tracked point A.

A total displacement of -165.288 mm is obtained at the end of the simulation. Figure 20 shows the isotropic deswelling of the actuator at the end of the simulation.

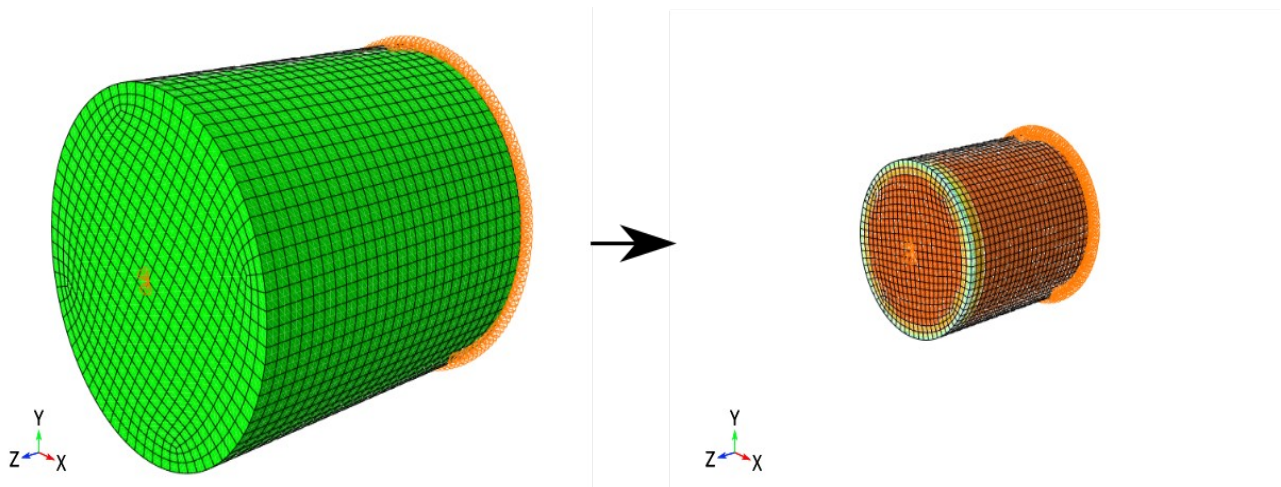


Figure 20: Actuator at initial state (left) and at final state (right).

The first immediate observation is that there exists a deviation of 0.17% in the simulation results from the required actuation length of 165 mm. However, the results fulfill the mechanical strain constraint given by equation (2.18). An important observation was the lack of experimental data in the model. While the expansion data was given for the temperature range of 32-36°C, the elastic modulus data was missing for the required temperature range. In lieu of this data, a constant value of 80 kPa was used for the material. This explains the source of error in the actuation length, as elastic modulus increases non-linearly with temperature. The results of this model can be easily improved, by supplementing it with more experimental data. As a future-work, the gel's elastic property should be improved to make it suitable for macroscopic application like the one in this thesis work. Also, more experimental data needs to be collected to accommodate a much wider range of operating temperatures.

3.2 Design of the outer shell

The description of the concept design for the tripod, detailed in chapter 1., talks about the outer shells which will contain the hydrogel actuator. With the determined dimensions of the actuator geometry, it is possible to find the required dimension of the outer shell. The total volume of the system of water and hydrogel remains constant throughout the process. The water is entirely inside the swollen actuator while at the deswollen state, the expelled water along with the shrunken gel occupies the volume inside the shell. Conservation of the volume gives the following equation:

$$\frac{\pi h_0 d_0^2}{4} = \frac{\pi h d_{shell}^2}{4} \quad (3.1)$$

where, h_0 and h are the initial and final height of the actuator during the actuation (deswelling) process. d_0 is the initial diameter of the actuator and d_{shell} is the inner diameter of the shell.

Equations (2.19) and (3.1) results in

$$d_{shell} = (1.4) \cdot d_0 \quad (3.2)$$

$$d_{shell} = 420 \text{ mm}$$

Contrary to the concept design, the final design shown in figure 21 has an inverted assembly. In the final design assembly, the upper shell-segment is made to overlap the lower shell-segment, such that the upper segment slides over the lower segment when deswelling occurs in the actuator. This change in the arrangement was required so that there is no obstruction to shell movement during actuation, thereby eliminating unwanted error. Since the expelled water accumulates in the lower segment during deswelling, it would have blocked the downward motion of the flanged upper segment in the concept

design. In the new assembly, there is no interaction between the accumulated water and the upper segment. Moreover, the water movement is also eased and directed due to this change.

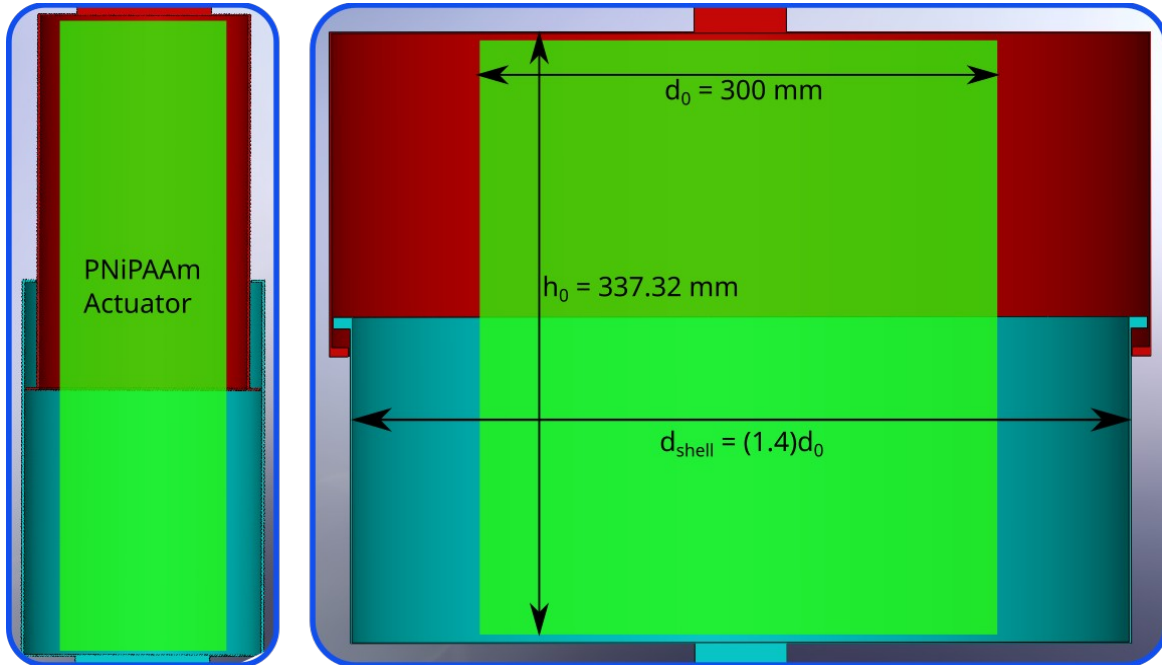


Figure 21: Left: Cross-section of concept design; Right: Cross-section of final shell design.

3.3 Tripod: Elephant-leg design

With the determined dimensions of the actuator and its shell, the CAD model was redesigned. Figure 22 shows the final model of the tripod designed in this thesis work. Due to the soft hydrogel material, the dimensions of the actuator to support the given load (just from the camera, without additional lens) are relatively large. This resembles to a medical condition called *Elephantiasis* and therefore it is named as Elephant-leg tripod.

Aesthetically and ergonomically, the design is poor and impractical. The innate weak mechanical properties of the PNiPAAm gel combined with quite conservative design constraint criteria, lead to such a bad design. However, this is a proof-of-concept work and some respite can be given to its visual appeal. Nonetheless, it reveals the fact that the mechanical properties of the material are unoptimized for this application, despite of the feasibility of the design.



Figure 22: Final tripod design: Elephant-leg Tripod.

3.4 Determinacy and Stability

A body at equilibrium is said to be stable, when it is kept in that pose by some supports such that they nullify the body's tendency to move as well as the loads acting on the body. Such a body will not perform translational as well as rotational motion, regardless of the applied load.

A body or system of bodies at rest is said to be determinate, if all the reaction forces and moments can be calculated using the equations of static equilibrium. The total number of reaction forces and moments should be equal to the degree of freedom of the system. For example, for a planar system the total number of forces and moment should not exceed 3. If the count of reaction forces and moments exceeds the degree of freedom of the system, then the system is said to be over-constrained (but stable) and indeterminate. On the other hand, if the count is less than the degree of freedom of the system, then the system is under-constrained (and unstable) and indeterminate.

Having defined the two terms, a conventional tripod is a stable and determinate structure. However, the tripod designed in this thesis has the ability of actuation. Therefore, while it becomes a structure when the swelling equilibrium is reached, it acts as a mechanism during the swelling (actuation) process. Since, there are two possible states of the tripod,

therefore we have to consider two cases, viz. (i) tripod as mechanism and (ii) tripod as structure.

- i. Tripod as mechanism – For this case, the tripod can be viewed as a mechanism of three links, namely the platform, the upper leg-segment of the actuated leg and the rest of the tripod structure (or ground). Figure 23 shows the setup in the CAD model. The topology plan of the mechanism is also drawn in the figure. When the first link and the last link in the system of bodies is ground, then joints cannot form a closed-loop (Woernle 2011). Hence, the joint in the red circle acts as a constraint to break the loop. Also, since the other two revolute joints are coaxial, therefore one of them becomes redundant. This results in degree of freedom equal to one for the system of bodies (or tripod mechanism). Equation (2.15) constrains the coordinate of the prismatic joint to that of the revolute joint (in red circle).

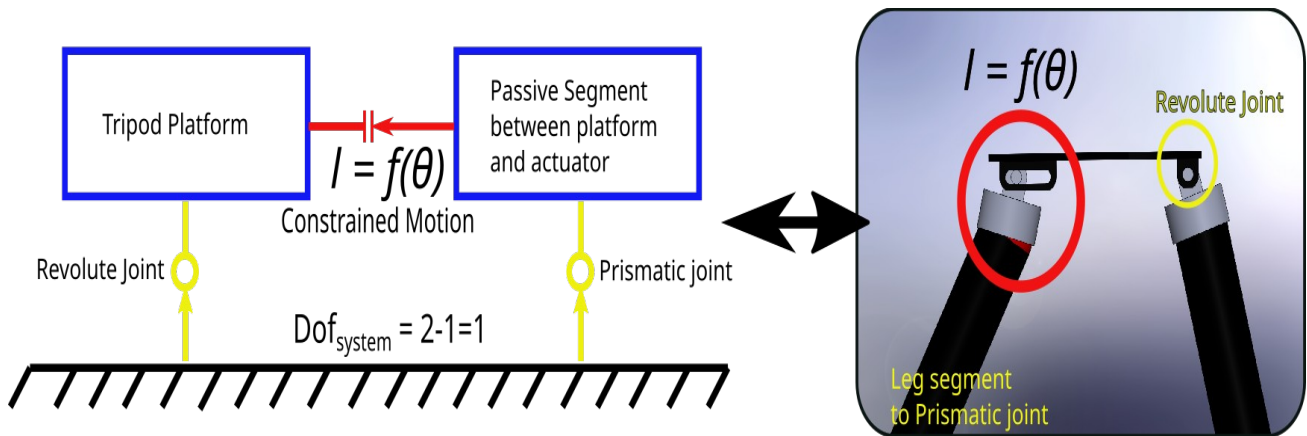
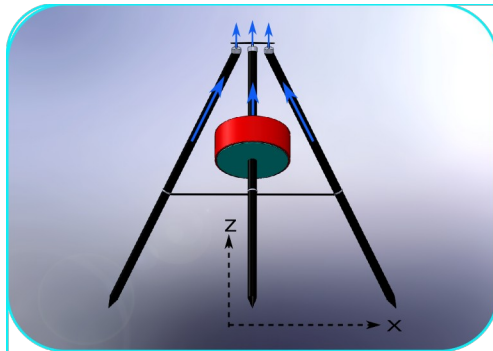


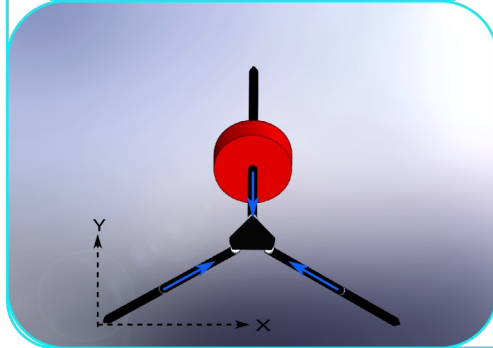
Figure 23: Topology plan of tripod mechanism.

- ii. Tripod as structure – When the swelling in the actuator reaches equilibrium, the actuated-leg essentially acts as a single rigid (approximately) leg for the applied load. Hence, this tripod acts as a conventional tripod. The tripod structure is 3-dimensional, giving it six degrees of freedom. There are three vertical reaction force components and three horizontal ones. Hence like a typical tripod, this tripod is also stable and determinate. Likewise, for each individual leg (acting as a planar body in this setup), there are three planar reaction components. Figure 24 summarizes the stability and determinacy of the tripod structure and individual legs.

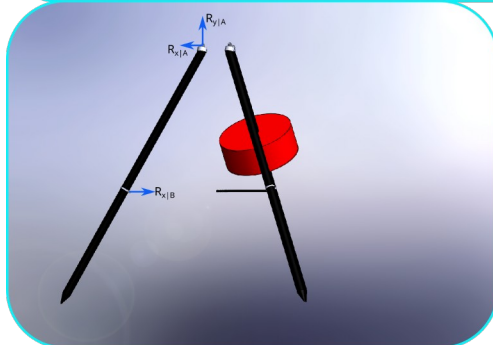


$$\text{DoF}_{\text{structure}} = 6$$

No. of reaction force components = 6



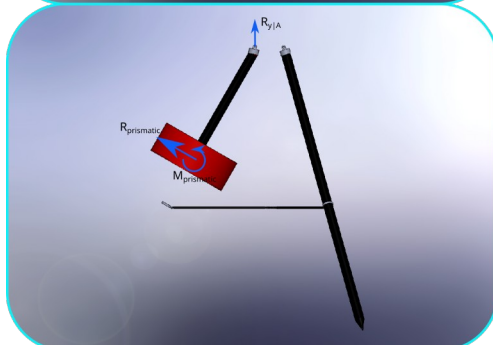
Stable & Determinate



$$\text{DoF}_{\text{leg}} = 3$$

No. of reaction forces = 3

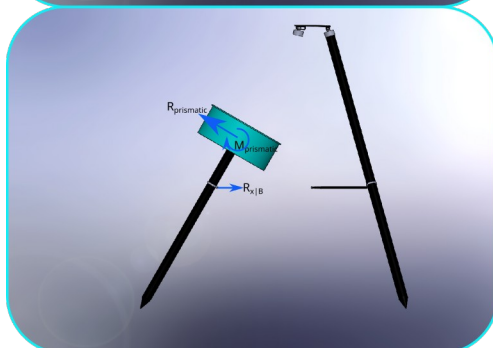
Stable & Determinate



$$\text{DoF}_{\text{segment}} = 3$$

No. of reaction forces = 3

Stable & Determinate



$$\text{DoF}_{\text{segment}} = 3$$

No. of reaction forces = 3

Stable & Determinate

Figure 24: (Top two blocks) 3D Tripod structure and forces; (Middle) Normal leg and it's forces; (Last two Blocks) The segments of the actuated leg and the reaction forces acting on it.

3.5 Actuation in the tripod mechanism

With the designed mechanism and the determined constrained motion equation, the *MATLAB Symbolic Toolbox* (The MathWorks Inc., 2022) code was written to simulate the actuation and animate the output of the tripod mechanism. The same was done with the tripod assembly modelled on *Solidworks* (Dassault Systèmes SolidWorks Corporation, 2022). Figure 25 is a collection of snapshots from both animations taken at an interval of 15° .

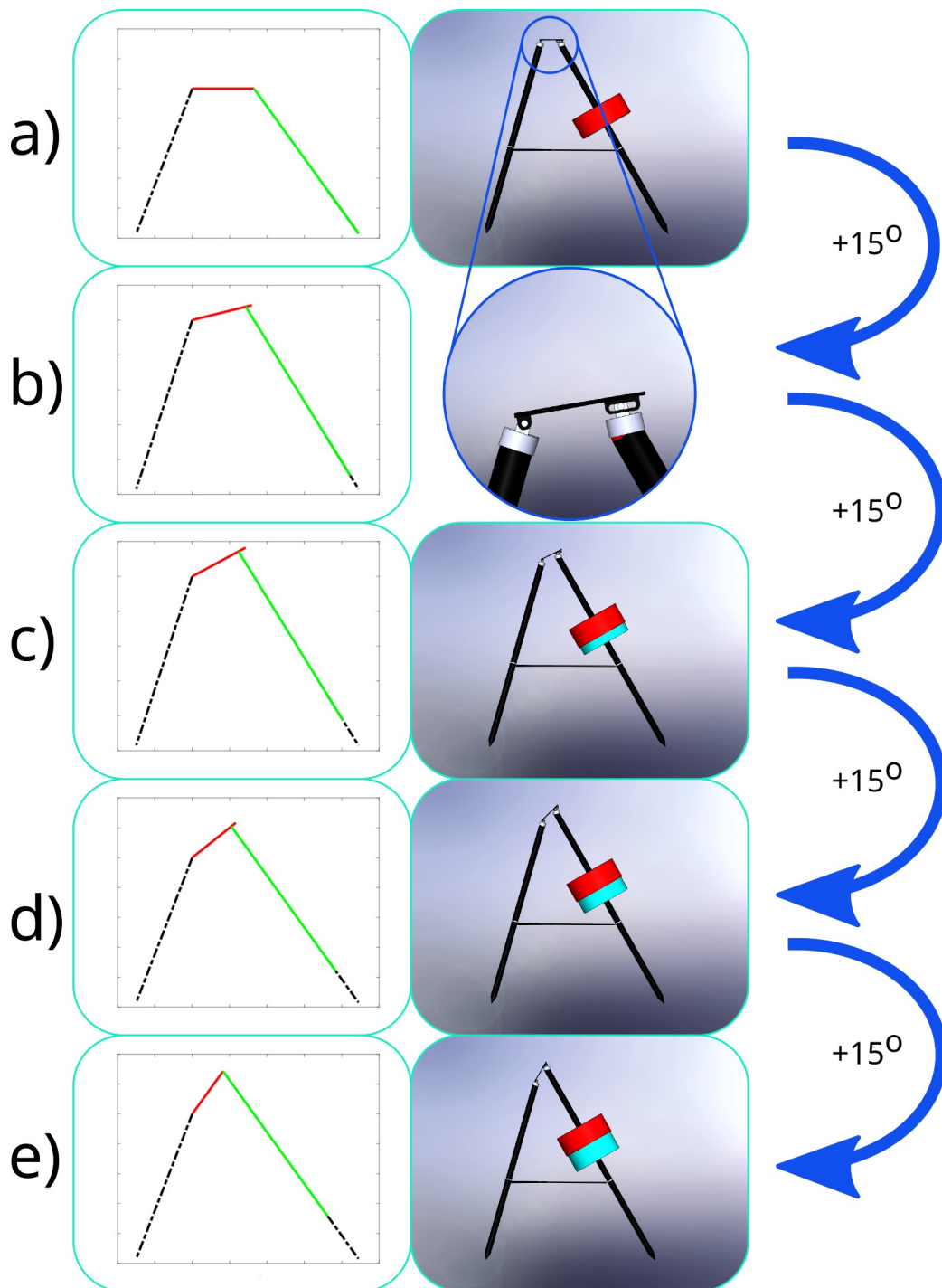


Figure 25: Actuation in tripod mechanism.

3.6 Maximum deflection due to bending, and Critical load for buckling

Having determined the diameter of the actuator, the bending and buckling phenomena can be studied for the given loads. Substituting $d_0=300$ mm in equations (2.21) and (2.23) results in

$$F_{cr}=11.0362 \text{ kN}$$

$$\delta_{max}=0.368 \text{ mm}$$

As evident a very large critical load is required to induce buckling in the actuator. Even though the elastic constant is relatively small for the hydrogel, the dependence of critical load on the fourth power of the diameter makes up for the low elastic modulus. The same is true for the deflection equation, where the maximum deflection value is inversely proportional to fourth power of diameter, when the span length is kept constant. The safety criteria for the beam deflection problem as given in equation (2.24), gives the span length as, $L=250 \times \delta_{max}$

$$L=91.88 \text{ mm}$$

which is much smaller than the actuator height. It is quite palpable that bending and buckling phenomena are dominated by geometric factors. The negative effects of poor mechanical properties of PNiPAAm on tripod design, were neutralized by the geometry of the actuator, at least for these two phenomena.

3.7 Kinetics of the designed actuator

The swelling kinetics model equations (discussed in section 2.2.2) can be used to estimate the time that the hydrogel geometry needs, in order to give a desired actuation (swelling/deswelling). Having determined the dimensions of the actuator needed for the tripod, the equations can be used to estimate the time it will take to elongate by 165 mm. The value of D_{coop} for PNiPAAm material, as determined in Krause (2016), is $3.8 \times 10^{-7} \text{ cm}^2/\text{s}$. Since the cylinder has a worm-like aspect ratio, therefore the radius of the actuator is used as the characteristic length for the calculations. From equation (2.4), the correction factor is

$$f=0.9631$$

Therefore the corrected diffusion coefficient $D_{exp}=f \cdot D_{coop}$ is calculated as,

$$D_{exp}=3.66 \times 10^{-7} \text{ cm}^2/\text{s}$$

Substituting D_{exp} and $r=15$ cm in equation (2.3) results in,

$$\tau = 6.229 \times 10^7 \text{ s}$$

Due to the asymptotic nature of logarithmic (and exponential) function, the fraction $\Delta r(t)/\Delta r_0 = 0.0001$, was taken as the realization of swelling equilibrium in equation (2.2) which yields

$$t = 54.268 \times 10^7 \text{ s}$$

As evident, the current actuator requires a very high amount of time to give the required elongation. This is in-line with the theory, since mechanical stability requirements lead to big dimensions of the actuator geometry. The swelling time is proportional to the square of the characteristic length. Due to the extremely small material property D_{coop} of PNiPAAm, it is unfeasible to realize an actuator design for astrophotography application. The available techniques to make hydrogel kinetics faster are mostly based on the idea of reducing the characteristic length. This unearths the inherent lack of optimization in the material properties of PNiPAAm gel for macroscopic applications in engineering.

3.8 Constrained motion and strain-rate

As mentioned in section 2.7.1, there exist a constraint between the actuated leg and tripod platform. Equation (2.15) defines that constraint under which the tripod mechanism works. Figure 26 shows the plot of the constraint function.

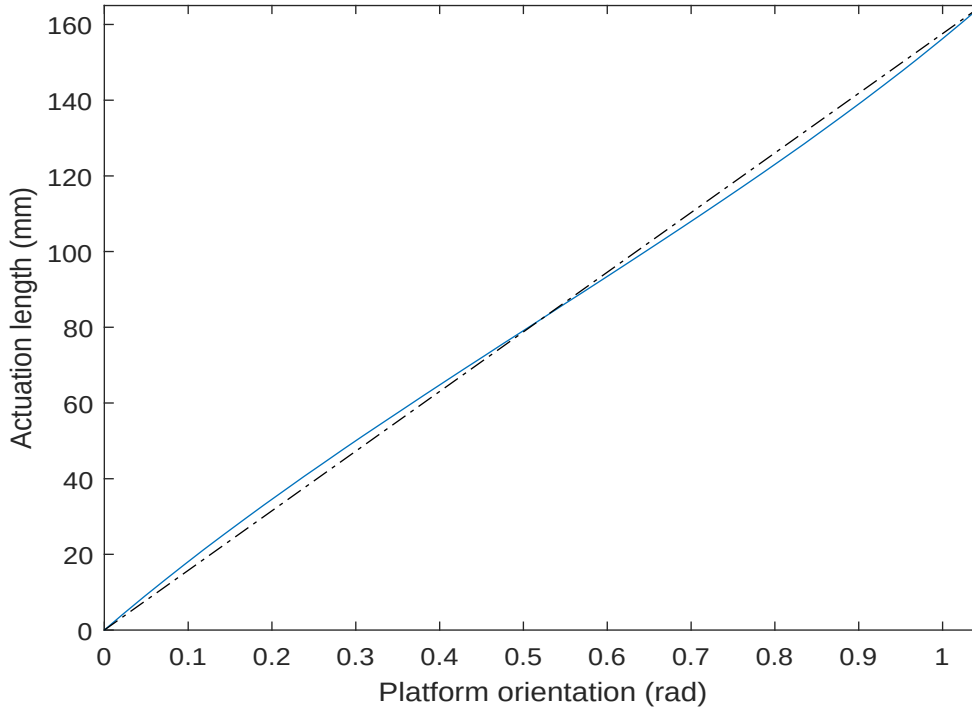


Figure 26: Constraint Function.

Since it is a non-linear function, therefore the function between strain rate of the actuator (or actuation rate) and angular velocity of the platform (which should be equal in magnitude to that of the earth's but opposite in direction) is an important aspect to consider. In general, the constraint equation can be expressed as:

$$l=f(\theta) \quad (3.3)$$

$$\frac{dl}{d\theta}=f'(\theta) \quad (3.4)$$

$$\Rightarrow \frac{dl}{dt}=f'(\theta) \cdot \frac{d\theta}{dt} \quad (3.5)$$

Substituting the value of angular velocity of earth as $d\theta/dt=\omega=7.2921 \times 10^{-5}$ rad/s and the function derivative in the above equation will give the required strain (or actuation) rate as a function of platform rotation angle. Figure 27 shows the function plot.

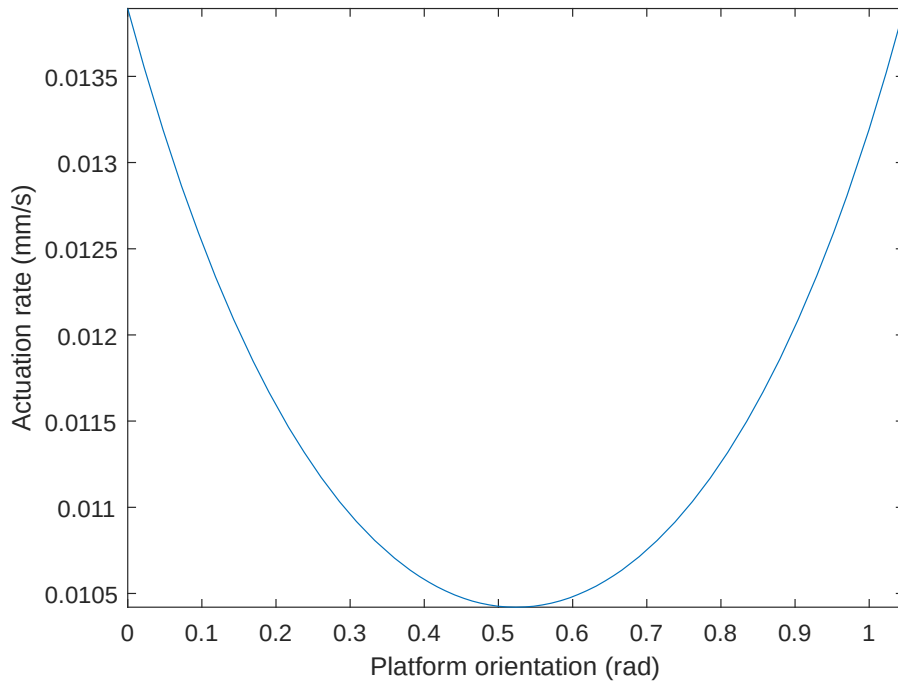


Figure 27: Strain rate of actuator as a function of rotation angle of the platform.

Given that the earth's angular velocity is constant, the actuation rate as function of time will be qualitatively equal to the above curve. However, literature shows that hydrogels

typically show a monotonically decreasing curve. Figure 28 depicts the strain rate v/s time curve of two different experimental studies.

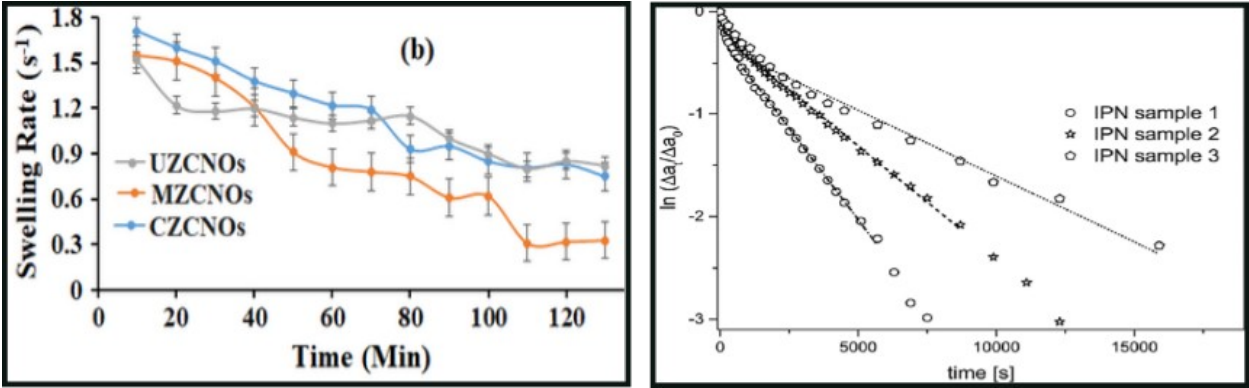


Figure 28: Hydrogel swelling rate curves. Image source: (Left) (Mamidi 2019) , (Right) (Krause 2016).

One possible solution of this problem would be to control the temperature change rate. Instead of applying the required temperature change in one step, the temperature of the system could be changed in steps. Depending on the desired derivative of the strain-rate versus time curve, the duration of individual steps can be modified. Although controlled heat transfer might be a potential solution, the extremely slow response time of the hydrogel material makes it vulnerable to failure. Therefore, in order to be able to get the precision for astrophotography application, the material or geometry should be modified to give a quick response.

4. Conclusion and Future-work

In the present thesis work, a tripod for astrophotography was designed and modelled. A commercially available approach to astrophotography includes an equatorial mount (among other mounts and accessories) and a tripod stand. The tripod is essentially a passive structure, which serves the sole purpose of providing stability during shots. However, to counter the earth's rotational motion and its effect in photos, additional mounts are deployed to give the required actuation. These mounts are heavy and expensive. This is where smart materials come into the picture as they provide an alternative option for actuation. Smart material like hydrogels, can be used to make structures which have the inherent property of actuation, eliminating the requirement of an external source of actuation.

Using this as a motivation, a tripod mechanism was designed in which one leg of the tripod contains a segment made of thermally-active hydrogel PNIPAAm material. This leg has the capability to elongate (or shorten), thus giving the actuation in the mechanism. This tripod mechanism thus provides a feasible and alternate approach to astrophotography.

This thesis work is a first attempt in this direction of hydrogel application and thus serves as a proof-of-concept. Therefore, imperfections and shortcomings can be anticipated. The output of the design process reveals two severe shortcomings in the concept design. Due to the hydrogel swelling kinetics and designed geometry of the actuator, the tripod fails to conform to the time constraint provided by the earth's angular velocity. The actuator takes an extremely long period of time to give the desired output. The second limitation is related with the actuation (strain) rate of the hydrogels. The earth's constant angular velocity combined with the constrained motion of the tripod mechanism gives an actuation rate which is qualitatively a parabolic curve. However, the experimental results in literature shows that hydrogels have an exponentially decreasing strain rate curve with respect to time. Thus, the tripod fails to produce a constant angular actuation for the camera.

Apart from these two, a less critical issue of aesthetics and ergonomics also arises in the current design. The source of these stems from the mechanical requirements. These issues prompt an optimization/ modification/ improvement of the material for this macroscopic application. Both, the mechanical properties and the swelling kinetics need to be customized to fix the above discussed design issues. Since, the prevalent methods of improving swelling kinetics inversely affects the mechanical properties, which are paramount for this kind of macroscopic use, therefore the material needs an overhaul at the chemistry level.

Apart from improving the material, there are some more design ideas to experiment in the future works. The first most natural idea is to manufacture circular hydrogel geometries capable of producing angular actuation. This will open entirely new and improved

approach to design the tripod. Another area of experiment is to embed the heating element within the actuator. This might improve the heat transfer rate as the area of contact for heat transfer will increase and also the distance to the heat source will also decrease. The swelling behaviour of such embedded hydrogels is an area of research. One more open front of experiment, is programming the micro-controllers for heat supply. As discussed in the current work, instead of changing the temperature at one go, it might be better to change it in successive steps of varying duration. This requires a separate research work to determine the temperature step-size based on the desired actuation (strain) rate for the astrophotography purpose.

5. References

D E Alexander. Nature's Machines: An Introduction to Organismal Biomechanics. (2017).

T Alfrey Jr, E Gurnee, W G Lloyd. Diffusion in glassy polymers. *Journal of Polymer Science Part C: Polymer Symposia* 12 (1966). [Link](#)

A Ashford. What is an autoguided? | BBC Sky at Night Magazine. (2022). Accessed on Sun, June 05, 2022. [Link](#)

M Banas. In-depth tripod review: Leofoto 'Summit' LM-364C. (2021). Accessed on Sun, June 19, 2022. [Link](#)

L C Dong, A S Hoffman. Synthesis and application of thermally reversible heterogels for drug delivery. *Journal of Controlled Release* 13, 21-31 (1990). [Link](#)

A Ehrenhofer, G Bingel, G Paschew, M Tietze, R Schröder, A Richter, T Wallmersperger. Permeation control in hydrogel-layered patterned PET membranes with defined switchable pore geometry – Experiments and numerical simulation. *Sensors and Actuators B: Chemical* 232, 499-505 (2016). [Link](#)

A Ehrenhofer, M Elstner, T Wallmersperger. Normalization of Hydrogel Swelling Behavior for Sensoric and Actuatoric Applications. *Sensors and Actuators B: Chemical* 255 (2018). [Link](#)

A Ehrenhofer, S Binder, G Gerlach, T Wallmersperger. Multisensitive Swelling of Hydrogels for Sensor and Actuator Design. *Advanced Engineering Materials* 22 (2020a). [Link](#)

A Ehrenhofer, T Wallmersperger. Hydrogels for engineering: Normalization of swelling due to arbitrary stimulus. 1016321 (2017). [Link](#)

A Ehrenhofer, T Wallmersperger. Shell-Forming Stimulus-Active Hydrogel Composite Membranes: Concept and Modeling. *Micromachines* 11 (2020).

P J Flory, J Rehner. Statistical Mechanics of Cross-Linked Polymer Networks I. Rubberlike Elasticity. *The Journal of Chemical Physics* 11 (1943a). [Link](#)

P J Flory, J Rehner. Statistical Mechanics of Cross-Linked Polymer Networks II. Swelling. *The Journal of Chemical Physics* 11 (1943b). [Link](#)

P J Flory. Network Structure and the Elastic Properties of Vulcanized Rubber. *Chemical Reviews* 35 (1944). [Link](#)

P J Flory. Principles of polymer chemistry. Ithaca, N.Y. : Cornell University Press, (1953).

K A George, E W Byrne, D J T Hill, A K Whittaker. Investigation into the Diffusion of Water into HEMA-co-MOEP Hydrogels. *Biomacromolecules* 5 (2004). [Link](#)

G Gerlach, K F Arndt. Hydrogel Sensors and Actuators: Engineering and Technology. (2010). [Link](#)

Y Jian, B Wu, X Yang, Y Peng, D Zhang, Y Yang, H Qiu, H Lu, J Zhang, T Chen. Stimuli-responsive hydrogel sponge for ultrafast responsive actuator. *Supramolecular Materials* 1, 100002 (2022). [Link](#)

A T Krause, S Zschoche, M Rohn, C Hempel, A Richter, D Appelhans, B Voit. Swelling behavior of bisensitive interpenetrating polymer networks for microfluidic applications. *Soft Matter* 12, 5529-5536 The Royal Society of Chemistry, (2016). [Link](#)

Laing O'Rourke. The Mathematics of Simple Beam Deflection. *The Royal Academy of Engineering*. Accessed on Sun, June 12, 2022 [Link](#)

Y Li, T Tanaka. Kinetics of swelling and shrinking of gels. *The Journal of Chemical Physics* 92 (1990). [Link](#)

D Malin, D D Cicco. Astrophotography – The Amateur Connection, The Roles of Photography in Professional Astronomy, Challenges and Changes. (2009). Accessed on Sun, June 05, 2022. [Link](#)

N Mamidi, G Ortiz, I L Romo, E Barrera. Development of Functionalized Carbon Nano-Onions Reinforced Zein Protein Hydrogel Interfaces for Controlled Drug Release. *Pharmaceutics* 11, 621 (2019). [Link](#)

T R Matzelle, G Geuskens, N Kruse. Elastic Properties of Poly(N-isopropylacrylamide) and Poly(acrylamide) Hydrogels Studied by Scanning Force Microscopy. *Macromolecules* **36** (2003). [Link](#)

H Mazaheri, A Ghasemkhani. Analytical and Numerical Study of the Swelling Behavior in Functionally Graded Temperature-sensitive Hydrogel Shell. *Journal of Stress Analysis* 3 (2019). [Link](#)

Mylivell. Mylivell Aquarium Heater for 5-10 Gallon Mini Fish Tank, Submersible Auto Thermostat Heater for Small Turtle Tank, Heaters for Fish Tank and Turtle Tank (50W). *Amazon.com* (2021). Accessed on Thu, June 23 , (2022). [Link](#)

J Newton, P Teece, H S Hogg. The Guide to Amateur Astronomy. Cambridge University Press, 1995. [Link](#)

S F Ray. Scientific Photography and Applied Imaging. Focal Press, 1999. [Link](#)

M Seuss, W Schmolke, A Drechsler, A Fery, S Seiffert. Core-Shell Microgels with Switchable Elasticity at Constant Interfacial Interaction. *ACS Applied Materials & Interfaces* **8** (2016). [Link](#)

M Shibayama, M Morimoto, S Nomura. Phase Separation Induced Mechanical Transition of Poly(N-isopropylacrylamide). *Macromolecules* **27** (1994). [Link](#)

M Shibayama, T Norisuye. Gel Formation Analyses by Dynamic Light Scattering. *Bulletin of the Chemical Society of Japan* **75** (2002). [Link](#)

M Shibayama, T Tanaka. Volume phase transition and related phenomena of polymer gels. 1-62 In *Responsive Gels: Volume Transitions I*. Springer Berlin Heidelberg, (1993). [Link](#)

Singularity. 2289-2289 In *Encyclopedia of Continuum Mechanics*. Springer Berlin Heidelberg, 2020. [Link](#)

Y Sun, X Zhao, W R Illeperuma, O Chaudhuri, K H Oh, D J Mooney, J J Vlassak, Z Suo. Highly stretchable and tough hydrogels. *Nature* **489**, 133-6 (2012).

T Tanaka, D J Fillmore. Kinetics of swelling of gels. *The Journal of Chemical Physics* **70** (1979). [Link](#)

T Tanaka, L O Hocker, G B Benedek. Spectrum of light scattered from a viscoelastic gel. *The Journal of Chemical Physics* **59** (1973). [Link](#)

T Tanaka. Gels. *Scientific American* **244**, 124-36, 138 (1981).

A Winkler, A Ehrenhofer, T Wallmersperger, M Gude, N Modler. Soft robotic structures by smart encapsulation of electronic devices. *Procedia Manufacturing* **52**, 277-282 (2020). [Link](#)

C Woernle. Mehrkörpersysteme: Eine Einführung in die Kinematik und Dynamik von Systemen starrer Körper. Springer Berlin, Heidelberg, 2011. [Link](#)

H Yuk, S Lin, C Ma, M Takaffoli, N X Fang, X Zhao. Hydraulic hydrogel actuators and robots optically and sonically camouflaged in water. *Nat Commun* **8**, 14230 (2017).